2008

Coded Pulse Transmission and Correlation for Robust Ultrasound Ranging from a Long-Cane Platform

Raymond S. Frenkel
University of Massachusetts Amherst, rfrenkel@ecs.umass.edu

CODED PULSE TRANSMISSION AND CORRELATION FOR ROBUST ULTRASOUND RANGING FROM A LONG-CANE PLATFORM

A Thesis Presented

by

RAYMOND S. FRENKEL

Submitted to the Graduate School of the
University of Massachusetts Amherst in partial fulfillment
of the requirements for the degree of

MASTER OF SCIENCE IN MECHANICAL ENGINEERING

February 2008

Department of Mechanical and Industrial Engineering
University of Massachusetts, Amherst

CODED PULSE TRANSMISSION AND CORRELATION FOR ROBUST ULTRASOUND RANGING FROM A LONG-CANE PLATFORM

A Thesis Presented

by

RAYMOND FRENKEL

Approved as to style and content by:

_____

Robert Gao, Chair

_____

Karl Jakus, Member

_____

James Mead, Consulting Member

_____

Mario A. Rotea, Department Head

Mechanical and Industrial Engineering

ACKNOWLEDGEMENTS

I wish to acknowledge and express my appreciation for the guidance, shared experience, and general mentoring of my research and academic advisor, Professor Robert X. Gao. His patience and insight and research acumen help me succeed in this effort.

I also wish to thank my colleagues in the Electromechanical Systems Lab for all their assistance, their encouragement and their friendship. Zhaoyan Fan for his assistance with graphics, Abhijit Ganguli for his review of this thesis, Sripati Sah, Cheng-Tai Yeh, M. Harris Hamld, Shuangwen Sheng, Li Zhang, and Rajesh Luharuka. The contributions and efforts of the various undergraduate students including Matthew Atwood, Gregory H. Meyerhoff, Patrick Regan, Thorsten Schlingmann, Lindsey Bellini, Stacy Canepari, and M. Patricia O'Brien, who contributed to this research through their honors projects, independent studies, design projects or as work studies were also greatly appreciated. Many thanks also go to Richard Winn of the MIE student machine shop, who did all the machining of the long cane components and helped to secure materials. All the professional staff of the Department of Mechanical and Industrial Engineering deserves mention for all their help.

Special acknowledgements are due Professor Karl Jakus and Dr. James B. Mead who served as committee members and Professor Sigfrid Yngvesson, Director of the Terahertz Laboratory in the Department of Electrical and Computer Engineering at The University of Massachusetts at Amherst who allowed me to use their facilities and equipment to assemble and test the circuit board for the prototype cane. Freescale, Sanyo, Maxim, Paragon and Newark, who supported this project with samples.

Finally, I must acknowledge the loving support of my wife, Margaret.

ABSTRACT

CODED PULSE TRANSMISSION AND CORRELATION FOR ROBUST ULTRASOUND RANGING FROM A LONG-CANE PLATFORM

FEBRUARY 2008

RAYMOND S. FRENKEL, B.S., UNIVERSITY OF MASSACHUSETTS

M.S., UNIVERSITY OF MASSACHUSETTS

Directed by Professor Robert X. Gao

The objective of this research was to increase the independence and safety of the sight impaired by developing an enhanced travel aid in the form of a sensor embedded long-cane to reduce the risk of injury from walking into suspended or overhanging objects while providing the sight impaired community with a familiar and well accepted tool. Prior research at the Electromechanical Systems Laboratory had established a theoretical framework for ultrasound-based ranging and spatial obstacle localization from the moving reference frame of a long-cane. A prototype was implemented using analog threshold detection techniques.

This research focused on a new approach. A coded pulse was transmitted and correlation techniques were used to identify echoes and determine time of flight. Compared to the prior effort this new approach was more sensitive, had greater noise immunity, and provide greater spatial resolution for obstacle detection. The first step in the coded pulse approach was to generate a transmit pulse with an embedded binary code that is highly distinguishable. A transmit pulse generated by phase modulating a 40 kHz carrier signal with a 13-bit Barker code word, with each bit consisting of 4 cycles of the 40 kHz carrier was used. Digitized representative echoes were used as reference vectors for correlation to account for the effect of the impulse responses of the transducers, the air, and the

reflection, on the transmitted pulse. In a detection cycle, the coded pulse was transmitted, the A/D converters took 2600 samples at the 150 kHz sampling rate to capture any echoes from objects between 1 and 4 meters in front of the cane. The receiver data was cross-correlated with the stored echo image to find echoes in the received signal. The correlation peak positions from the upper receiver were then compared to the peak positions from the lower receiver and if they collaborated within the synthetic aperture, the range and height were calculated annunciation was made by a synthesized voice. The new obstacle detection system described above was designed and a prototype was constructed and embedded into the shaft of an 18 mm diameter body of a long cane.

TABLE OF CONTENTS

Page

Page

Page

LIST OF TABLES

Table Page

LIST OF FIGURES

Figure Page

Page

CHAPTER 1

INTRODUCTION

The objective of this research was to investigate ultrasonic ranging techniques to enhance the performance of the sensor embedded long-cane travel aid for the sight impaired. The long cane, as the most widely used and accepted travel aid of the sight impaired, leaves its users at risk of sustaining head and upper body injury from collision with protruding or suspended obstacles [1]. The long-cane can feel the nature of a path and detect holes, curbs, steps, and obstacles on the ground, however, as Figure 1 shows, suspended or protruding obstacles above waist height cannot be detected with a traditional long-cane. Hanging plants, tree branches, and guy wires are just a few of the common obstacles that can injure the user of a long cane. This limitation can be corrected by embedding an electronic collision warning system into the body of a long cane to detect such obstacles, while maintaining the platform that is well accepted by the sight impaired community. Embedding an ultrasonic sensor system into a long-cane will reduce the risk of injury from walking into suspended or overhanging objects while providing the sight impaired community with a familiar and well accepted tool. Prior research efforts have shown the feasibility of this solution [2]. The challenge was to achieve the robustness and reliability necessary to be of practical use.

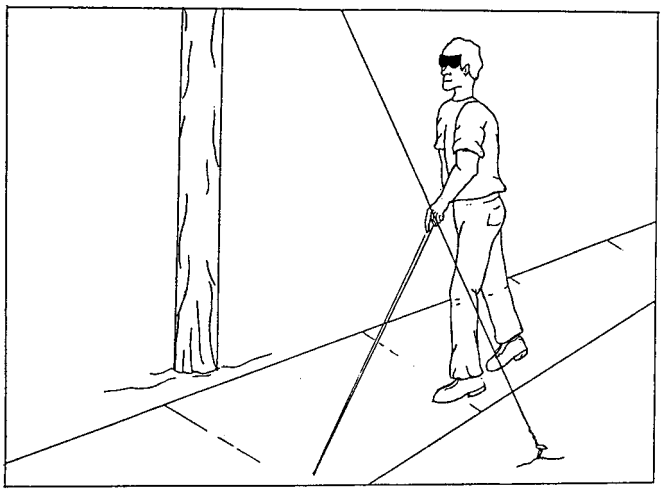

Figure 1: Limitations of the traditional long-cane.

The significance of this research is illustrated by the size of the population that stands to benefit. According to the American Foundation for the Blind [1] there are approximately 10 to 11 million blind and visually impaired people in North America and every seven minutes, someone in America will become blind or visually impaired [3]. In 1994-95, 8.1 million people were estimated to have a functional limitation in seeing and there were approximately 1.3 million Americans who reported legal blindness (a rate of 5 per 1,000). There are 130,000 users of the long-white cane in North America alone. With the increase of the elderly population and Macular Degeneration, this figure is expected to double by 2015. The long-white cane is the most popular and accepted travel aid for the visually impaired community. According to the estimates of the World Health Organization [3], there are some 180 million people worldwide today with visual disability and between 40 and 45 million persons are blind and cannot walk about unaided.

1.1. Present State of Knowledge in Electronic Travel Aids

Research efforts aimed at developing Electronic Travel Aids (ETAs) to enhance the mobility of the visually impaired can be traced back to the early 1960s. A wide range of ETAs have been developed that can be used alone or in conjunction with primary aids such as guide dogs or long-canes [4]. Only the most significant examples are presented here.

Most ETA's can be grouped into one of two categories: environmental sensors or clear path indicators [4]. Environmental sensors attempt to compensate for lost vision by providing spatial information to functioning senses such as hearing or touch. This 'alternate vision' using functioning senses is to enable the visually impaired to perform like sighted people. Clear path indicators acknowledge that many blind persons can travel independently without using any electronic aid and therefore only provide limited information to supplement and interact with their already highly developed mobility skills.

1.1.1. Environmental Sensors

Environmental sensors use the sight impaired user's functioning senses (auditory or tactile) to create a virtual mental image of the space ahead. The problem is the signals produced are complex and difficult to interpret, and interfere with the direct sensing of the environment. A typical example is the *Sonicguide* developed by *Leslie Kay* [4] which was a head mounted device resembling a pair of glasses with a sensing range up to 5 meters within a field of view of approximately 50°. The device sensed the reflected fraction of the emitted ultrasonic beams and transposed the ultrasonic frequency into the audible spectrum. The resulting signal heard through an earphone was a complex sound

pattern containing information about the distance, direction and the surface characteristics (hard or soft, rough or smooth, etc.) of the obstacles from which the ultrasonic energy was reflected [6]. Comparisons in a real world setting between blind pedestrians using the Sonicguide along with the long cane and those who used long cane only demonstrated a measurable improvement by the Sonicguide users in terms of orientation, reduction of bodily contacts with obstacles and continuousness of walking. However, evaluations from psychologists, mobility teachers and blind people have shown that the signal produced by the Sonicguide was difficult to interpret, required special training to apply effectively, and masked direct environmental cues [7].

Jorgensen patented a hand held echo location system [8] which delayed the received echo to improve perception. He utilized a hand held ultrasonic emitter, which could be pointed in any direction and a microphone to receive the echoes. The echo signal was stretched over time to make them interpretable and then converted to an audible frequency signal the user could hear. Together with the attenuated initial burst, this stretched echo enabled the user to construct a mental picture of the obstacles in the direction pointed in. While technically successful, this had the disadvantage of disrupting the ordinary hearing of the user. Also the cost was potentially high.

Similarly, Ifukube et al [9] designed and built an echo location device modeled after that of the bat. The device was located on a pair of eyeglasses and used down swept FM sounds from 70 to 40 kHz, emulating the location method used by most bats. The signals were picked up by a two channel receiver, processed into 8192 sampling points, and then converted into an audible signal. Testing has demonstrated that a user can perceive fine

objects (a few millimeters in size) at a range of 1 meter. However, this device also obstructs the user's normal hearing of the environment.

1.1.2. Clear Path Indicators

Clear path indicators provide a simple "go" or "no-go" warning signal indicating whether or not it is safe to proceed along the path of travel. This class of mobility aid is generally used in conjunction with other primary aids such as the long cane or a guide dog. A true clear path indicator only provides the minimum information necessary to indicate an obstruction. Typical examples of this type of aid are the Nottingham Obstacle Detector (NOD), the Mowat Sensor, the Sonic Pathfinder, and the Laser Cane.

The *Nottingham Obstacle Detector* (NOD) is a pocket-sized, flashlight (torch) shaped, hand-held unit that radiates ultrasonic pulses in a narrow beam about 2 meters ahead of the user [10]. Eight musical notes were used to indicate the distance to the nearest obstacle within this range. No special training was needed to use the device. However, it was found that the tones tended to drift resulting in possible misinterpretations and the device required active scanning by the user. The tones were also difficult to distinguish in a noisy environment and the unit provided no information as to the height or size of an obstacle.

Hoydal and Zelano's work [11] appears to be relevant in spirit to the Nottingham Obstacle Detector. They directly applied a Polaroid ultrasonic ranging system [12], and used an audible signal with a frequency inversely proportional to the distance of the target as output. Tests were conducted on two blind individuals who confirmed the general sensing capability of the device under normal environmental conditions.

However, since the "flashlight-like" device is mounted in a PVC tube that must be hand held, its use interferes with the use of a long-cane which may limit its acceptance by the blind community.

The *Mowat Sensor* was a hand-held ultrasonic device that was based on the "sing-around" principle [13]. The device detected the closest object in a four-meter range and indicated the distance by vibrating, the higher the vibration frequency, the shorter the distance. Vibration of the device body in the range of 10-40 Hz was used to indicate the target's distance. Similar to the NOD, this device was simple to use, and the cost was relatively low. However, blind users in evaluations did not favor the use of vibration as an indicator of distance, since it caused bodily fatigue.

The *Sonic Pathfinder* is a further development of the NOD, this ultrasonic aid is mounted on a spectacle frame and could sample the environment about 2.4 meters ahead of the user within an arc of 120° [13]. Similar to NOD, descending notes of the major musical scale were used as an audible indication of the decreasing distance to the target as the user approached. The aid was easy to use, required no special training, and, since it was placed at the eye height, it provided much better head protection than the NOD or the Mowat sensor. Like other aid devices mentioned above, the Sonic Pathfinder must be used in conjunction with the long cane, due to the simple nature of its output signals.

The *Laser Cane* resembled the form of a long cane with a thick upper section into which three laser sensors were mounted. The laser cane used the triangulation principle to scan obstacles within three areas ahead of the users: obstacles lying on the travel path ahead, those above chest height, and discontinuities in the road surface (e.g. step downs). Like a conventional long cane, the tip of the laser cane scanned in an arc across the travel path in

synchronism with the forward motion of the user. Three audible signals of 200, 1,600 and 2,600 Hz were used to identify and display potential dangers within the three areas respectively [4]. Evaluation by blind pedestrians showed that although the signals were simple in nature, a relatively long period of learning under the supervision of professional instructors was required to handle the cane effectively. This long training period as well the very high price (more than $2,000 apiece) and the special maintenance and service required has prohibited the laser cane from gaining popularity.

The above cited efforts have not produced a widely accepted and functional travel aid for the sight impaired community. These early devices lacked good functionality, interfered with the use of the reliable, traditional long cane, produce tones or beeps that distracted from listening to the environment, or were prohibitively costly. Research efforts at the University of Massachusetts Electro-Mechanical Systems Laboratory has been aimed at overcoming these deficiencies by creating a system that was easy to use, did not mask audible environmental cues, complemented the use of the traditional long cane, and was affordable. Prior research has made considerable progress in embedding a sensor system that detected obstacles not normally detected by the long-cane into a long-cane. The focus of this research is the investigation of coded-pulse and correlation techniques for ultrasonic ranging to improve the robustness of the embedded obstacle detection system. False alarms must be minimized while still providing a high level of obstacle detection. Not only must obstacles be detected, their threat must be assessed in terms of the detecting capabilities of the long-cane.

CHAPTER 2

BACKGROUND

Ultrasonic obstacle detection using signal processing techniques has been the subject of extensive research by the robotics community and has seen much advancement in the last few decades. The goal of this research was to investigate these technological advances for the purpose of enhancing the mobility and safety of the visually impaired. Making the technology compatible with a human user becomes a challenge. A robot's on board computer can processes a constant stream of sensor data but excessive information would not only be irritating to a visually impaired traveler, it would interfere with normal perception. The technology therefore, should not interfere with the user's auditory perception of the surroundings any more than what is absolutely necessary for safe navigation. This was accomplished by developing signal processing and target discrimination techniques to limit the reported obstacles to those that can not be detected by traditional use of the long-cane, and by discretely warning the user of detected obstacles with a short message via a synthesized voice (as opposed to continuous tones or beeps used by other systems). This technology was miniaturized and imbedded into the limited space of a long-cane.

2.1 Previous Work

Prior research at the Electromechanical Systems Laboratory (EMS) had established a theoretical framework for ultrasound-based ranging and spatial obstacle localization from the moving reference frame of a long-cane [2].

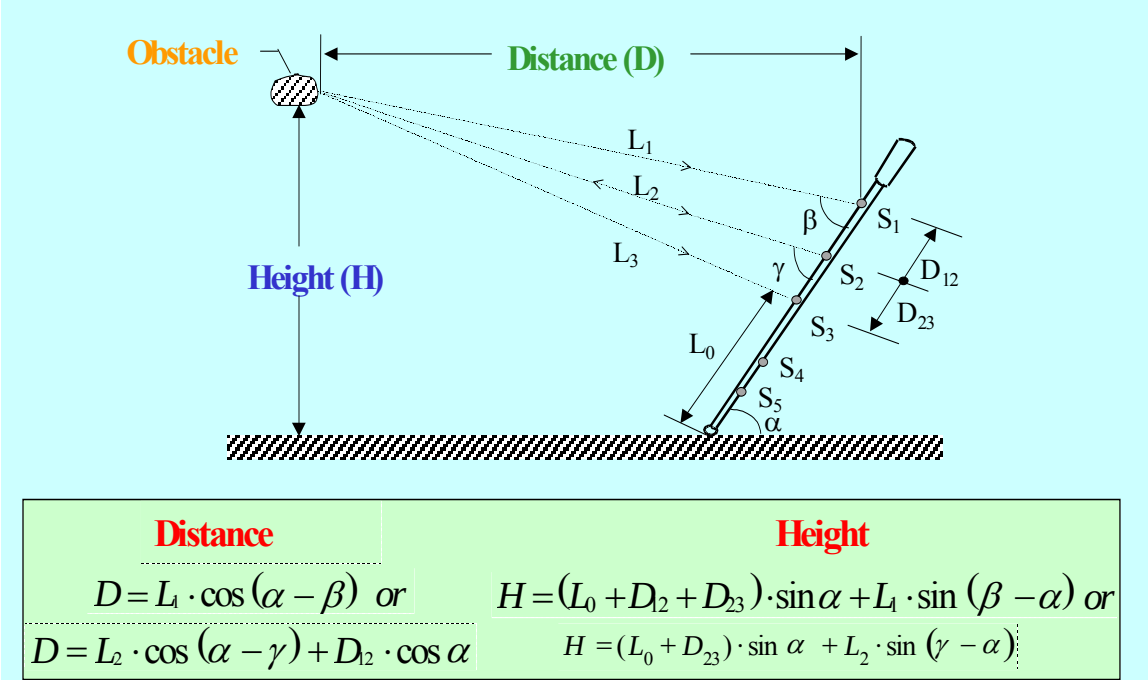

Figure 2: The measurement principal of the model.

An analytical model (Figure 2) was developed to calculate the distance and height of an overhanging obstacle using the geometric relationships between the obstacle, the three co-linear ultrasonic sensors (S_1 to S_3) mounted on the long-cane, and the inclination of the cane (angle α) as measured by a second set of sensors (S_4 & S_5) mounted on the lower side toward the tip of the long cane. The model assumed obstacles would reflect an ultrasonic pulse in a specular or light-like manner with the time between the transmitting of a pulse and the receiving an echo being proportional to the distance traveled by the pulse, as a function of the speed of sound in air. Using the geometrical relationships between an obstacle and the receivers, the obstacle would be identified as a wall, a point, or an irregular, undefined obstacle. Walls, which could be detected by conventional use of the long cane, were to be ignored and only point or irregular obstacles were to be reported by means of a synthesized voice.

This analytical model was used to design a proof-of-concept prototype. The effects of sensor spacing and cane vibration were studied as well as the error induced by cane movement and inclination. A sensor system based on a PIC microcontroller was successfully embedded into the 25 mm diameter aluminum cylinder that constituted the mid section of a cane shown in Figure 3. A wireless receiver displayed the transmitted ranging information using a synthesized voice. This demonstrated the ability to miniaturize the sensor system and embed it into a long-cane.

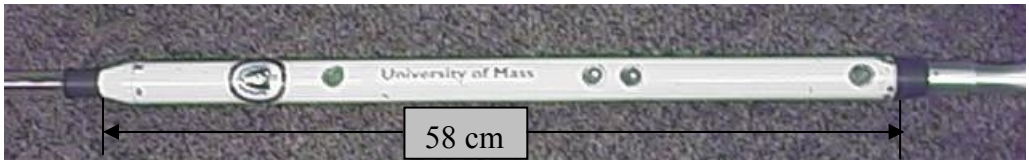

Figure 3: The mid section of the prototype cane.

The prototype cane suffered from a lack of robustness and false alarms. The design used threshold detection ultrasonic ranging which assumed the amplitude of a true echo would exceed the pre-determined detection threshold of the receivers. This assumption worked in a well-controlled laboratory environment with strongly reflecting obstacles. However, under less favorable conditions out on the street or walkway, signal echoes below the detection threshold and echoes buried in the noise were not detected, leading to false alarms. Multiple obstacles could not be distinguished since only the first echo above the threshold was detected. The detected echo at one receiver might not be from the same obstacle as the echo detected at another receiver. Frequent false alarms rendered the prototype cane unusable in realistic settings. To make the sensor embedded cane a practical mobility aid for the sight impaired, the robustness of the system had to be improved.

2.2. Present state of Knowledge in Ultrasonic Detection

H. Peremans et al added signal processing techniques used in radar and sonar systems [15] [14]to the model of acoustic imaging based on geometrical wave propagation by Kuc and Siegel [17]. They showed that three co-linear transducers, two receivers and one transmitter/receiver could be combined to form a high-resolution sensor array [16]. This sensor array was capable of determining both distance and bearing of all isolated objects in the field of view, and was able to discriminate between planes and edges. The digital signal processing techniques used started with the transmitted waveform. The center transducer emitted a pulse based on a 13-bit Barker code word with each bit (binary digit) consisting of 4 cycles of a 50 kHz carrier. The received signals from each of the three transducers were convolved with a matched filter to produce an autocorrelation function (ACF) of the transmit waveform. The correlated peak of the ACF determined the Time-of-Flight (TOF) and a list of echo arrival times for each receiver was generated. A matching algorithm based on the maximum likelihood principle matched the echo arrival times for a single object from each transducer list to form a list of triples. All target reflectors were assumed to be curved. The circle representing the surface of a reflector had to be tangent to each ellipse defined by the TOF calculated distance traveled by a pulse from the center transmitter-transducer to the reflector and back to an end receiver-transducer. It also had to be tangent to the circle defined by the TOF of a pulse from the center transducer back to itself. This geometrically defined the reflectors position and

radius of curvature. The radius of curvature was used to distinguish planes (walls) from edges.

Kleeman and Kuc presented a sonar array consisting of two transmitters and two receivers and established that this number is necessary and sufficient to distinguish planes, corners, and edges [18]. In this design the receivers were closely spaced to minimize correspondence errors for echoes received at the two receivers from the same object. An echo from an object detected at one receiver will arrive at the other within the TOF distance between the receivers. The smaller the distance between receivers, the smaller the interval that must be searched for a correlating echo at the other receiver, hence a reduction in processing load. The combination of two receivers was used to form a vector sensor which measures the range and bearing to a reflector. A linear model for the effects (impulse response) of transducers, excitation, incidence angles to the transducers, dispersion and absorption with distance of travel in air, and reflector properties was used to generate a matrix of templates of received pulse shape for discrete angles and ranges. Optimal arrival times were estimated using template matching from the stored echo shapes for different transmitting and receiving angles and ranges. When the correlation coefficient was below a threshold of 0.8, the arrival time estimates were rejected. Overlapping echoes and noise disturbances were thus rejected. The technique of correlating the received echoes between receivers as well as correlating to modeled wave forms should reduce false alarms from overlapping echoes and noise generated ghost objects.

Webb et al determined the range and angular position of an object by a time delay beam-forming technique to generate a two-dimensional array [19]. Delays were calculated

corresponding to each range and angular position. These were stored and added as appropriate to the received signals to form a two dimensional array. The dimensions represented range and angle and a peak in the array represented a target. The targets range and angular position were found from the position within the array of the maximum of the peak. Based on work done at Nottingham University, capacitive transducers were used, as opposed to the more common piezo-electric transducers. The capacitive transducers have a better impedance match to air and are therefore more efficient transmitters and more sensitive receivers but they are broadband compared to narrowband piezo-electric transducers and therefore more sensitive to noise.

CHAPTER 3

DESIGN OF A NEW SENSOR EMBEDDED LONG-CANE

3.1 Theoretical Background

3.1.1 Ultrasonic Ranging

Ultrasonic ranging is well suited to close range obstacle detection because of the specular nature of ultrasonic wave propagation, the relatively slow speed of sound, and the almost universal sound reflectance of all solid objects. The availability of small-scale transducers makes ultrasonic technology particularly attractive for integration into the body of a long-cane. Ultrasonic ranging works by measuring the time interval between the transmission of a pulse and the reception of an echo. The distance between the pulse transmitter and the wave reflecting object is obtained by multiplying the Time-of-Flight (TOF) by the speed of sound and dividing by two. The simplest method of detection uses a threshold detector that triggers when the first echo exceeding a preset threshold is received. A problem with this approach is that the first echo may not be from an object of interest. Also, objects that present a small profile will produce a weak echo that can be missed by this detection method. Increasing the energy level of the transmit pulse will increase the level of the echoes and thus their delectability, but poses technical challenges.

The energy content of a pulse is determined by its amplitude (A), frequency (ω),duration (t_p), and the density of the medium (ρ) as seen in Equation 1.

$$E = \rho\omega^2 A^2 t_p \tag{1}$$

The amplitude of a pulse is limited by the capability of the transducer, which is limited by size. Ultrasonic wave propagation in air is subject to exponential loss with increasing frequency, due to the compressibility of air, which limits the frequency range that can be used. This leaves increasing pulse duration as the principal means of increasing echo detectability. However, for a threshold detection system, when the pulse duration is increased, the echoes from closely spaced objects will overlap, making them indistinguishable. This reduces the spatial resolution of the system.

Both the problem of overlapping echoes and the energy level of the pulse can be overcome by introducing pulse compression, originally developed for RADAR, that makes high spatial resolution possible using longer pulses to allow for weaker echoes to be detected [20]. In pulse compression, a pulse with a distinctive pattern is transmitted and the starting position of the echo of this pattern in the received signal can be identified to calculate the TOF.

3.1.2 Ultrasound Pulse Coding (Correlation or Pulse Compression)

The key to pulse compression is correlation, a measure of the similarity between two signals. The correlation function identifies the location of one number sequence in another by giving the highest value when the search sequence is aligned with an image of itself in the sequence being searched. This reduces or compresses a sequence or pattern of numbers to just one location, namely the point of alignment. The advent of microcontrollers and digital signal processing (DSP) greatly simplifies the use of correlation techniques when compared to analog correlators. An analog signal is converted to a set of numbers by repeatedly sampling the signal at a sampling rate and

converting the instantaneous amplitudes to numbers. In using DSP for echo location, the received signal is time sampled to create a one-dimensional array of amplitudes, called the received signal vector. This vector is correlated with a vector containing the time samples of the signal being searched for, to produce a resultant vector containing the product sums of the received signal vector and a time shifted series of the search pattern as a correlation vector. Peaks in the resultant vector indicate the position of similarity in the signal vector to the correlation vector. The process is expressed mathematically in Equation (2) as:

$$c(l) = \sum_{i=0}^{N-1} e_i \cdot x_{i+l} \quad l = 0,1, \ldots N \tag{2}$$

where $c(l)$ is an element of the correlation vector, N is the number of samples in the signal, e_i is an element of the correlation vector, x_{I+l} is an element of the signal vector, and l is the lag or offset of the correlation vector.

Correlating a vector with itself is called autocorrelation. Ideally a vector used for correlation should correlate with an aligned image of itself and not with anything else, thus having a strong autocorrelation function (ACF). This ideal code word must be infinitely long so the ideal signal must have an infinite time-bandwidth product, with time being the duration of the signal transmission and bandwidth being the quantity of information the signal can convey per unit of time (e.g. bits per second). An infinite time-bandwidth product is not possible for a short duration pulse from a narrow band ultrasonic transducer. Both the narrow frequency response of a piezoelectric transducer and the length of the pulse limit the quantity of information a pulse from a piezoelectric transducer can contain. A coded pulse of short length from a narrow band piezoelectric

transducer will have an ACF consisting of a main lobe at zero time shift and secondary lobes, called sidelobes, at small time shifts on either side of zero shift showing some level of correlation at points of misalignment. However, some patterns produce a stronger correlation than others [21]. The binary code sequences with the highest ratio of aligned correlation (main lobe) to misaligned correlation (sidelobe) are called Barker Codes [22]. Barker Codes have the strongest ACFs for all codes up to 13 bits long, and by definition all the sidelobes of Barker Codes are 1, 0, or -1 [23]. A complete list of Barker codes is presented in Table 1 which shows that the longer codes produce higher autocorrelation amplitude and therefore can have a higher main lobe to sidelobe amplitude ratio than shorter codes [25] since correlation is a sum of products,.

To create a pulse with a strong ACF, the 13 bit Barker code sequence was embedded into the transmit pulse by means of phase modulation, shifting the phase of the signal 180^{o} between ones and zeroes as shown in Figure 4. However, since the piezoelectric

Table 1: The complete list of Barker Code binary sequences.

Length	Sequence	Sidelobe level (dB)
2	10 (or 11)	-6.0
3	110	-9.5
4	1011 or (1001)	-12.0
5	11101	-14.0
7	1110010	-16.9
11	11100010010	-20.8
13	1111100110101	-22.3

ultrasound transducers used for long cane embedment cannot respond to single cycles of a phase reversal but takes several cycles for the oscillations to reach maximum amplitude after the application of an excitation and several cycles to stop oscillating after excitation

ceases, four cycles of a 40 kHz carrier were used for each binary digit as shown in Figure 5.

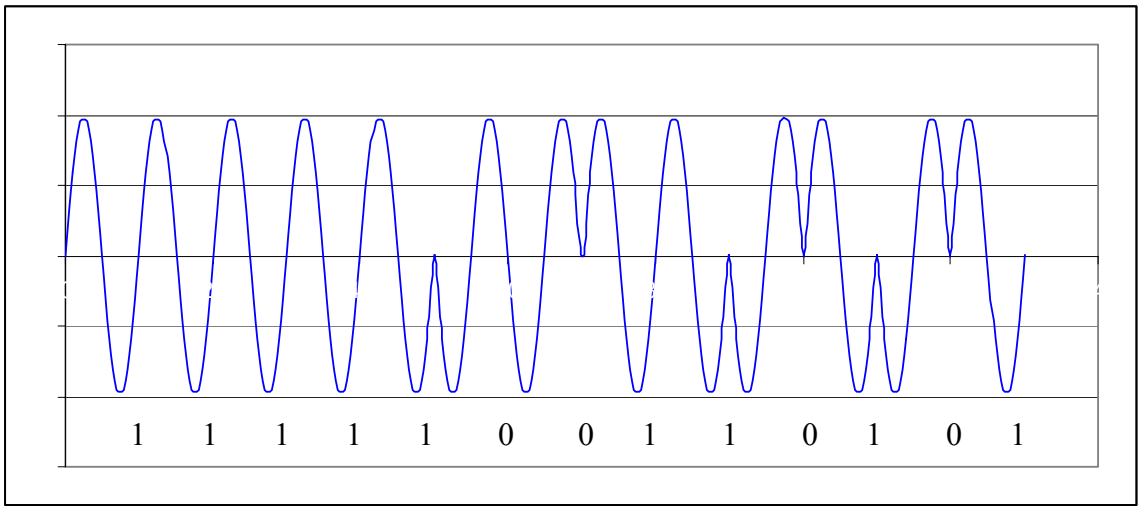

Figure 4: 13 Bit Barker Code (1 cycle per bit)

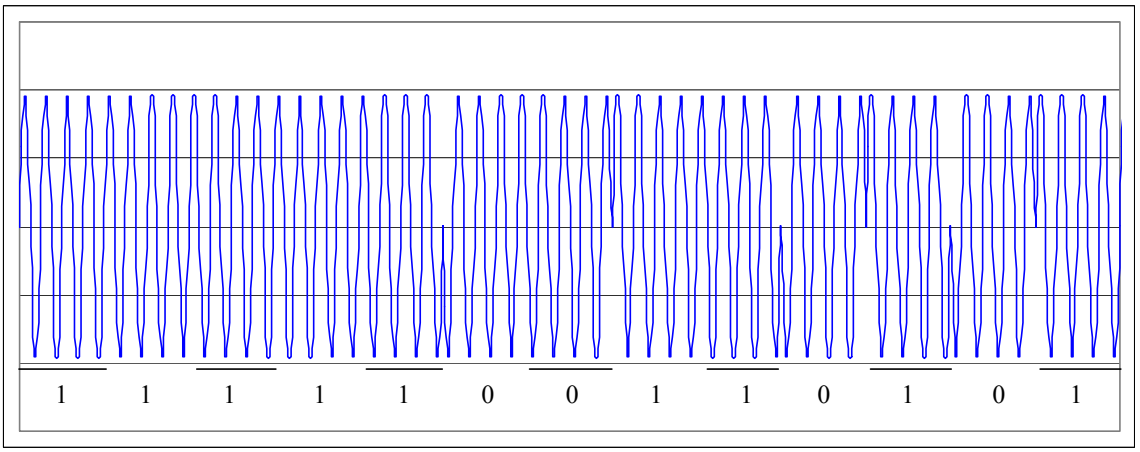

Figure 5: 13 Bit Barker Code (4 cycles per bit)

This is because piezoelectric transducers are inherently narrow band devices and using four cycles per bit reduces the coding frequency to 10 KHz, which is in the -20dB bandwidth of the transducers and produces a distinctive pulse of 52 cycles. Figure 6 shows the sensitivity of the receivers and the sound pressure level of the transmitter as a function of frequency.

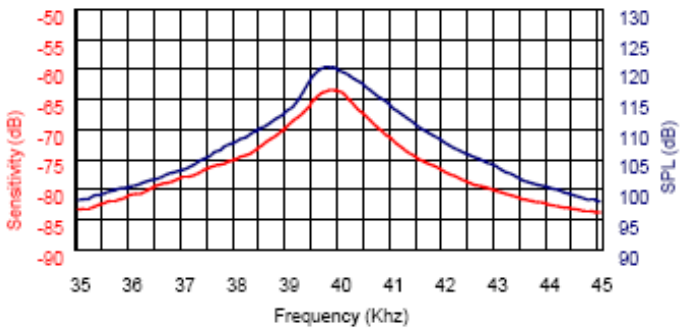

Figure 6: Frequency response of transducers [24]

Lowering the frequency of the encoding would lower the distortion but would lengthen the pulse beyond the minimum detection range desired. Since we are not trying to de-code the received pulse but only trying to accurately determine the TOF, four cycles per bit ensures at least four cycles of excitation before a phase change to accommodate the constraint of the transducers and is a good compromise.

The electrical pulse used to excite the ultrasound transmitter cannot be used as a search pattern or correlation vector to search for echoes in the received signal, because the filtering effect of the transducers and air on the pulse signal has to be taken into account [26]. In the presented study, the correlation vector was generated from a digitally sampled high signal-to-noise ratio echo signal from a large target [27]. Such a vector is shown graphically in Figure 7 along with its ACF. The peak of the autocorrelation for the pulse in Figure 7 is more than five times the surrounding sidelobes and close to twenty times the correlation to noise. Using this pulse and applying correlation to the received signal, the TOF for all echoes received after a pulse transmission was determined by locating the correlation peaks with an iterative peak-finding algorithm. Figure 8 illustrates the iterative process used to locate the correlation peaks.

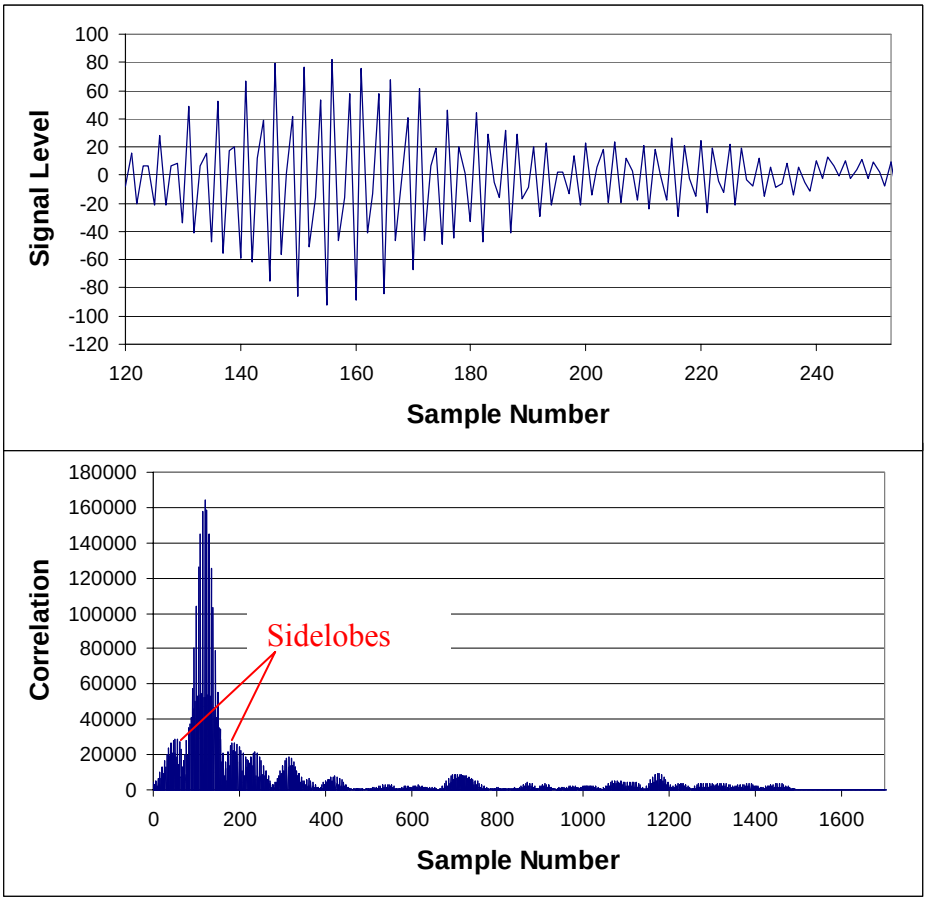

Figure 7: An encoded pulse and its autocorrelation.

In a typical environment where the long cane is used, not every ultrasound echo represents a threat. Obstacles above the head would not pose a collision hazard while those below the waist height would be detectable by normal use of the long cane. That leaves a range of obstacles between waist and head height that constitute reportable collision hazards. In this study the range of between 0.9 m and 2.0 m above the floor is used as the range for reportable collision hazards [28].

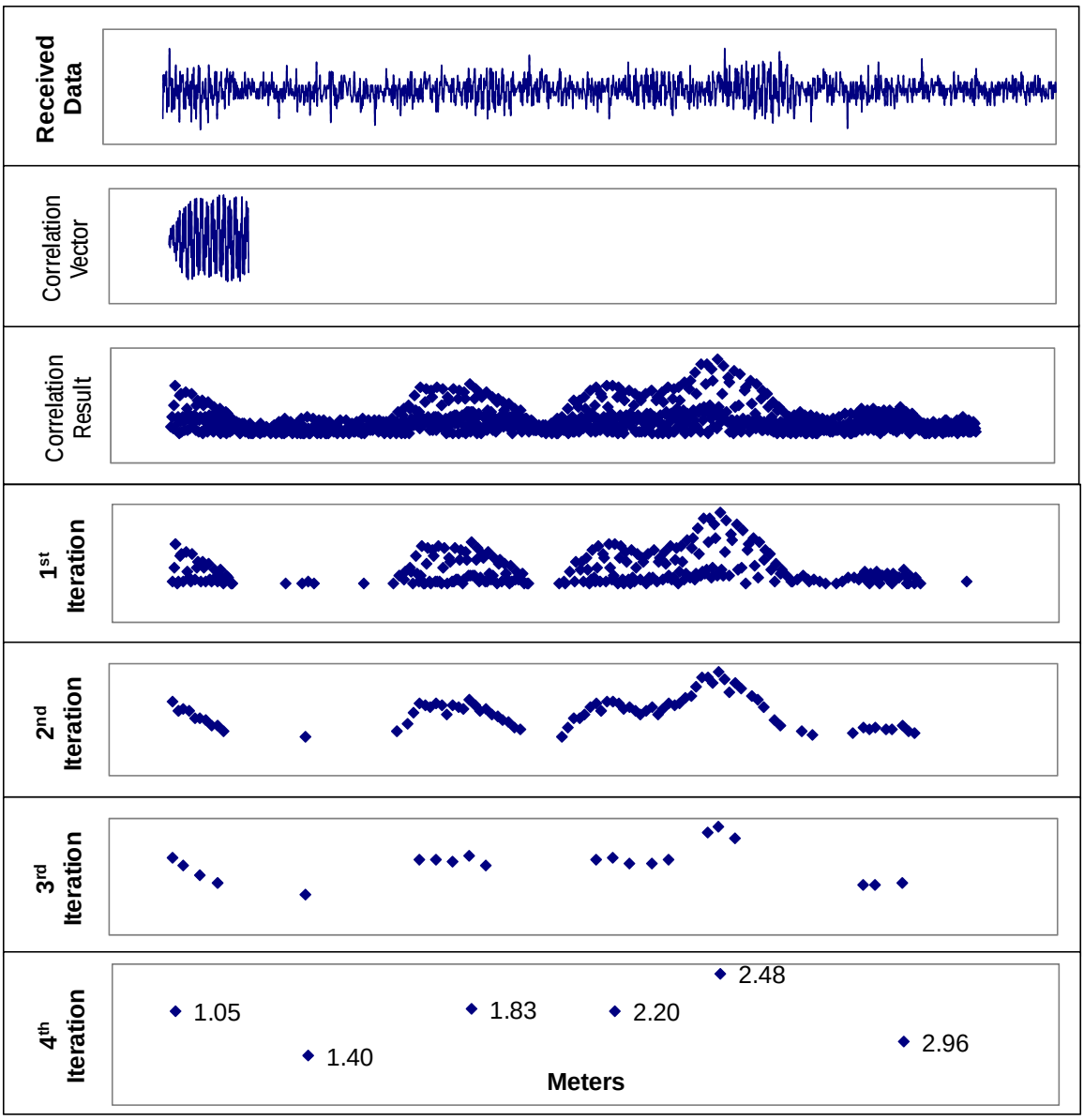

Figure 8: The iterative peak location process.

3.1.3 Synthetic Aperture

The height of an echo source can be determined by triangulation, if two receivers are spaced along the body of the long cane [29]. From Figure 9 it can be seen that the TOF_1 for ultrasound Receiver 1 is the time the pulse takes to travel the distance a + c and TOF_2 to travel b + c. An echo from an object on the plane that is the perpendicular bisector of

the line joining the two receivers will arrive at both receivers at the same time (TOF_1-TOF_2=0). An echo from above that plane will arrive at the upper receiver first and an echo from below that plane, as shown, will arrive at the lower receiver first. The fixed spacing between the receivers determines the maximum TOF difference (TOF_1-TOF_2) that an echo returning from a particular obstacle can have. The maximum difference in TOF occurs when the obstacle is on the line connecting the two receivers. If for a correlation peak from Receiver 1 there does not exist a corresponding correlation peak from Receiver 2 that is within this maximum difference, the correlation peak is un-collaborated and geometrical calculations cannot be performed. With a fixed spacing between the two receivers that is small compared to the distances being measured, the difference in the TOF from the two receivers is given as:

$$\Delta t = \frac{d}{c} \cdot \sin(\eta) \tag{3}$$

where Δt is the difference in TOF, d is the distance between the receivers, c is the speed of sound in air, and η is the angle between the line perpendicular to, and bisecting, the line connecting the two receivers and the line from the bisect point to the obstacle. This TOF difference can be used to discriminate by obstacle position. The relative location between correlation peaks of the two receivers in the time domain indicates the height of an obstacle. The maximum and minimum height of interest can be calculated in terms of Δt by replacing the obstacle in Figure 9 with the upper and lower boundaries of the synthetic aperture in Figure 10 and calculating Δt as a function of distance. This yields a range in Δt that varies with distance because the angle η for a constant height varies with distance.

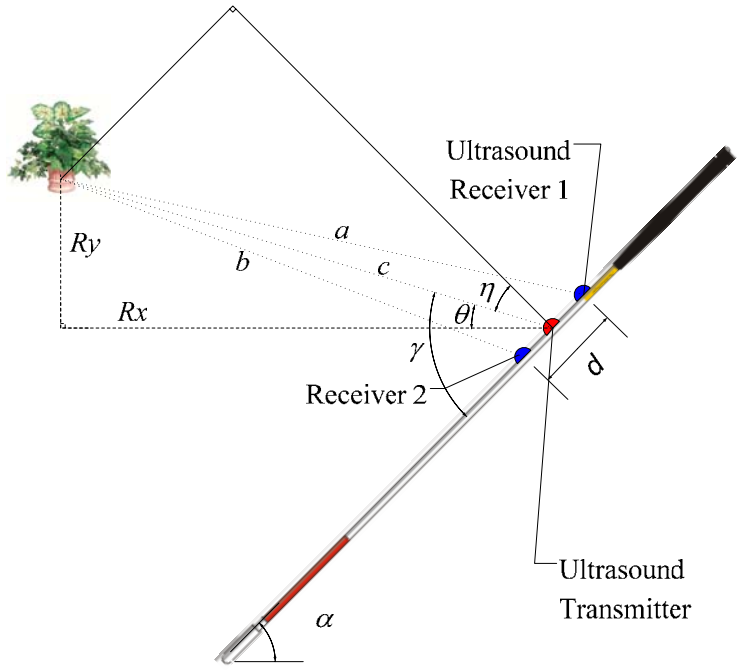

Figure 9: Geometry of Sensor System

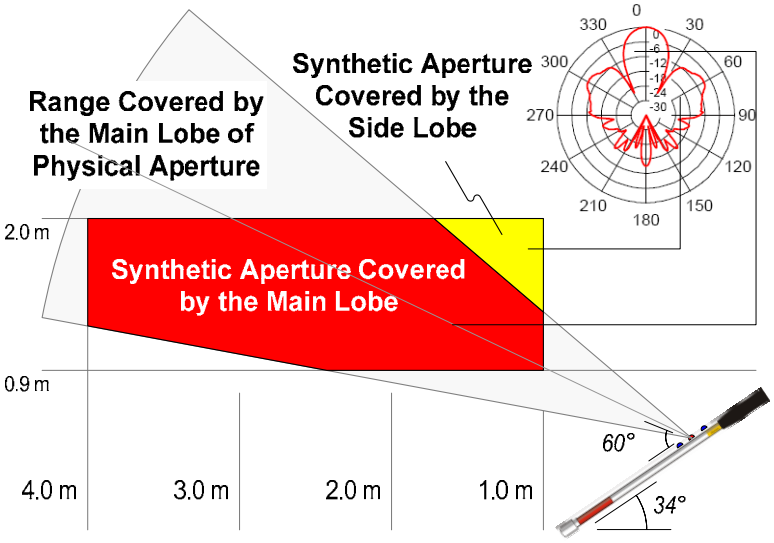

Figure 10: Synthetic aperture boundaries.

This range in Δt for the two receivers constitutes a synthetic aperture in one dimension, in line with the two receivers, and represents a range of the angle η for which only obstacles

that pose a collision threat, obstacles above 0.9 meters and below 2 meters are detected. The range of Δt to reject obstacles below 0.9 meters and above 2 meters, as a function of distance, is also a range in the difference of the sample number position of the correlation peaks for the two receivers since sample number is directly related to time. Using sample number position simplifies the calculations, because sample number is the native 'unit' to the microcontroller. Equation (4) shows the relationship of time t, to the sample number:

$$t = (\text{Sample \#}) \times (\text{Sample Period}) \tag{4}$$

To derive equations to calculate the boundaries of the synthetic aperture in terms of Δt, the values of Δt for 0.9 meters and for 2 meters were plotted against the TOF for Receiver 1, using a sampling period of 6.667 υs, as shown in Figure 11. The choice of sampling period is discussed in section III.

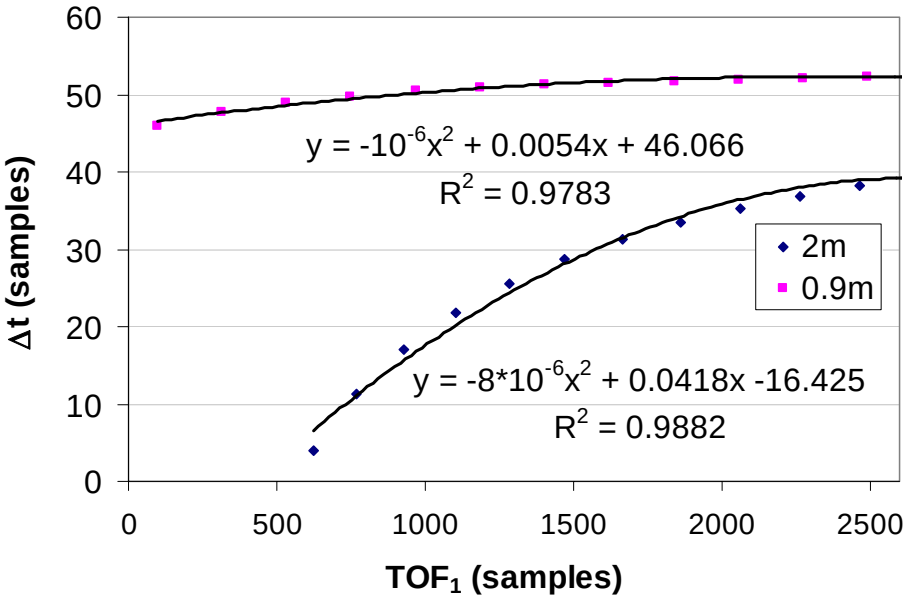

Figure 11: Calculation of the boundaries of the synthetic aperture.

Second order polynomial trend lines were fitted to the curves to get Equations (5) and (5):

$$u = -8^{-6} \cdot a^2 + 0.0418 \cdot a - 16.425 \tag{5}$$

$$l = -10 \cdot 10^{-6} \cdot a^2 + 0.0054 \cdot a + 46.066 \tag{6}$$

where a is the TOF as a sample number of the correlation peak from Receiver 1, u is the upper boundary of Δt for the synthetic aperture, and l is the lower boundary of Δt for the synthetic aperture.

Equations (5) and (6) calculate the upper and lower boundaries of Δt in samples and form the test for the synthetic aperture:

$$l \geq \Delta t \geq u \tag{7}$$

3.1.4 Elevation and Range Calculations

If Equation 7 is true, there is a collision hazard to report. The range or horizontal distance would then be calculated and reported to the user. Referring to Figure 9, the timing, in samples, of a correlation peak from receiver 1 represents the distance from the transmitter to the obstacle, c, plus the distance from the obstacle to the receiver, a. A correlation peak from receiver 2 represents the distance c plus the distance b. The distance between the receivers, d, is small relative to a, b, and c and the transmitter is half way between the receivers so c can be calculated as:

$$c = \big((c + a) + (c + b)\big) / 4 \tag{8}$$

The angle between c and the perpendicular bisector of the receivers, η, is calculated as:

$$\eta = \sin^{-1}\left(\frac{\left((a+c)-(b+c)\right)}{d}\right) \tag{9}$$

With η, the angle made by c with the horizontal, θ, can be calculated as:

$$\theta = \frac{\pi}{2} - \alpha - \eta \tag{10}$$

Using θ, the distance, R_x, and height, R_y of the obstacle, relative to the transmitter, can be calculated as:

$$R_x = c \cdot \cos(\theta) \quad and \quad R_y = c \cdot \sin(\theta) \tag{11}$$

Adding the height of the transmitter gives the actual height (H) of the obstacle as:

$$H = R_y + 1.25 \cdot \sin(\alpha) \tag{12}$$

where: 1.25 m is the distance from the tip of the cane to the transmitter. The synthetic aperture eliminates the need to perform complex geometrical calculations that would otherwise be needed to locate and identify an obstacle, thus reducing the computational load by eliminating the need to calculate the range and height for all detected echoes. Obstacles outside the aperture are ignored. Any correlation peak from one receiver that does not have a collaborating peak from the other receiver within the range of the synthetic aperture will be rejected as an aberration from noise or as coming from a source outside the area of interest. Neither of these constitutes a collision threat.

3.2 Design Strategies

3.2.1 Mechatronics approach for sensor-integrated cane development

The design of the sensor embedded cane is multi-disciplinary in nature. The cane shaft is a mechanical structure. The obstacle detection system is a combination of analog electronics, computer hardware and software. Both the mechanical and the software design must consider human factors engineering in order to produce an ergonomic design compatible with a sight-impaired user. And, the electronic and mechanical designs are interdependent; one has to accommodate the other.

The necessary synergy between design fields is embodied in the mechatronics design philosophy. The interaction between various components and subsystems need to be considered in a parallel fashion in order to achieve synergy. Potential conflicts need to be analyzed, and overall system performance must be optimized, at the system level. The mechatronics design philosophy is pictorially presented in Figure 12. This figure

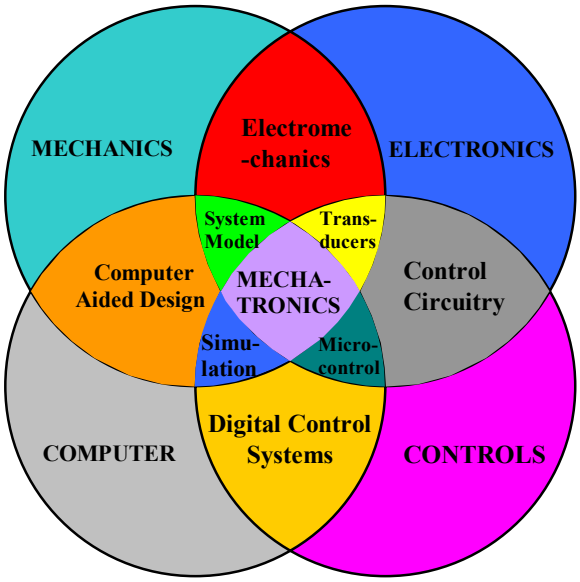

Figure 12: Mechatronics design concept [31]

illustrates the interaction between the traditionally separate disciplines encompassed by the sensor-embedded long-cane project.

For the sensor embedded long-cane, the electronic design depends on the mechanical design and vise versa. The design of each subsystem must be based on the synergy of all these technologies rather than on the requirements of each isolated individual discipline. This design interdependence is illustrated in Figure 13.

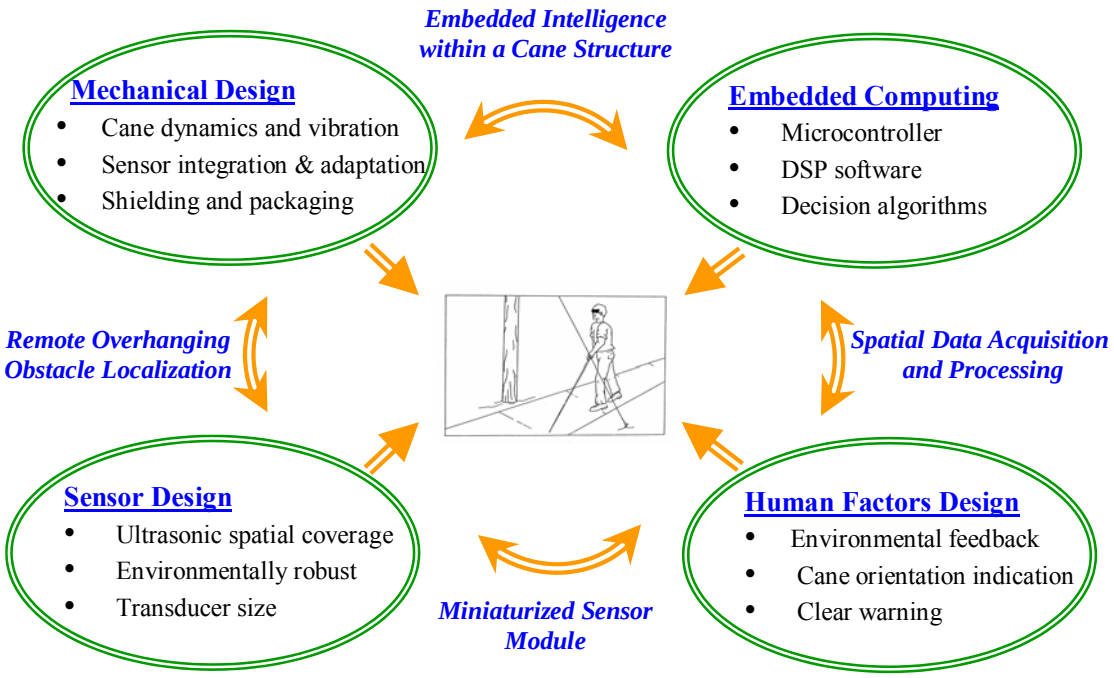

Figure 13: Mechatronics approach for sensor-integrated cane development.

In this illustration each oval represents a traditional technology. The items listed within the oval illustrate the major focus for the cane development in the corresponding field. The double arrows show the necessary integration between two particular fields. The unidirectional arrows demonstrate the necessary contributions of each field to the total design of the sensor embedded long-cane as an integrated system. Almost by necessity,

the mechatronics design philosophy will be adhered to in this research effort. The choice of sensor spacing is an example.

The sensor spacing not only impacts the mechanical design, the range and resolution of the sensor array, the processing load on the embedded processor and the circuit board design are also affected by the sensor spacing. The interactions are not always complementary. This forces trade-offs in the discipline specific designs in order to achieve the greatest efficiency in the overall design.

3.2.2 Requirements and design criteria

The sensor embedded long-cane must function in two ways. First, it must serve as a conventional long-cane. If it fails in this area the sight impaired community will not accept it. Second, it must give the user the spatial information needed to avoid collisions with suspended or protruding obstacles. These requirements are contradictory in that a long cane is generally lightweight, relatively small in diameter, inexpensive, and may fold up for storage or for traveling in a vehicle. The obstacle detection function requires space between sensors, computing power, and a source of energy, things that add weight, size, and expense. Mechatronic design requires both requirements to be considered though out the design process.

To serve as a conventional long-cane the weight, balance, and stiffness of the cane must match a traditional cane as closely as possible. A typical long cane has a length of between 105 and 155 cm, weighs less than 300 grams, and is approximately 20 mm in diameter at the handle. Figure 14 shows three typical rigid long canes.

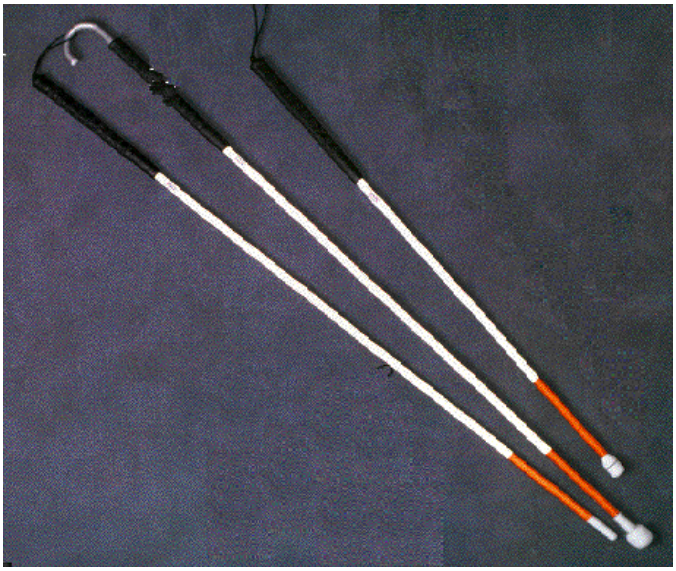

Figure 14: Three typical non-folding long canes.

The collision warning system must give accurate and timely warnings, without false alarms or overly interfering with the user's working senses.

For the initial design strategy the sensor embedded long-cane was divided into two logical subsystems, the electronic collision avoidance system and the cane body. The cane body was further subdivided into three functional sections, the handle, the upper body, and the lower body. The handle was given three functions, to comfortably fit the hand, to provide the user an index to orient the cane, and to hold the batteries. The upper body houses the electronic collision avoidance system. The transducers are mounted on this section and the supporting electronic circuits are contained inside this section. The lower body section completes the long cane structure and supports the rubber tip at the correct distance from the handle. The length of this section can be set by the needs of the user.

Customer need surveys indicated that high data quality (timely, accurate warnings) from the electronic collision avoidance system, low cost, and good long cane function of the

cane itself were the most important requirements followed by long operating time between battery charging. Good long cane function was decomposed into low weight, small diameter, and structural stability.

The functional requirements for data quality are the number of sensors used to collect data and the sophistication of the data analysis algorithm. The operating time depends on battery capacity, the number of sensors, and the processing power required to execute the algorithm. The weight of the cane is a function of the number of sensors, the battery weight, and the cane bodyweight. The structural stability of the cane body is controlled by the properties of the material used and the wall thickness chosen. The relationships and correlations between the customer requirements and the functional requirements are illustrated in the house of quality matrix shown in Figure 15. Solid circles in the matrix indicate a strong relationship between engineering design requirements and customer needs, open circles indicate some relationship, and blank squares indicate no relationship. The "roof" shows the correlation or interrelationship between design requirements. High positive correlation is indicated by circled plusses, positive correlation by plusses, and no correlation by blanks. The strategy employed was to categorize the customer and functional requirements as design variables or constraints, to model customer satisfaction as a function of the design variables (the constraints and their interactions) and to optimize the model for customer satisfaction.

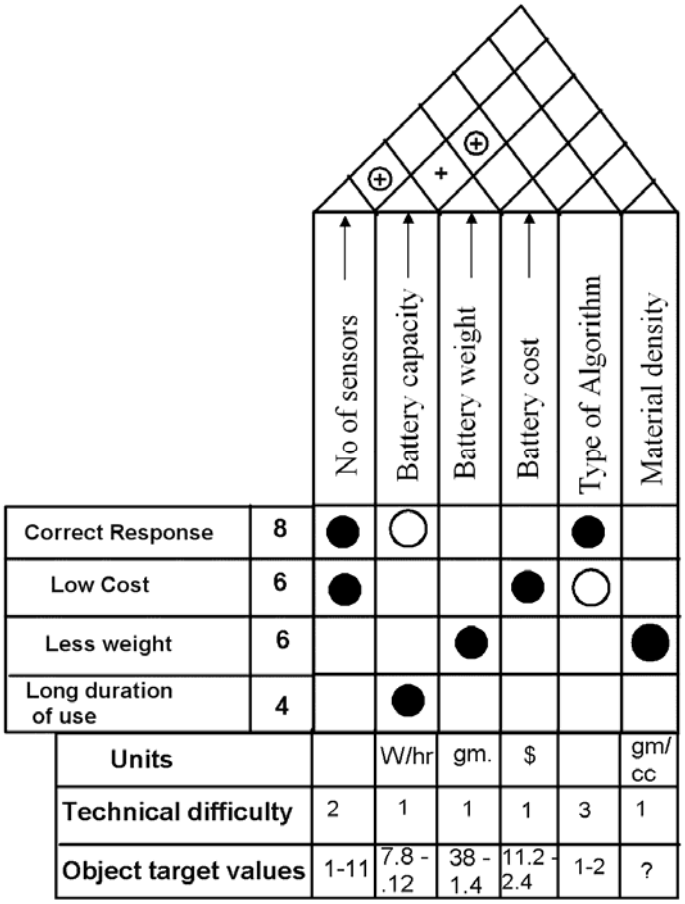

Figure 15: House of quality

3.2.3 Design Optimization

The function structure diagram for the sensor embedded long-cane (Figure 16) shows the distinct separation of the conventional long cane function and the function of the electronic collision avoidance system. As indicated above, the unrelated functions of the two systems were dealt with separately for the initial design even thought both functions contribute to the cane weight. The choice of materials for the cane body were made by analyzing a standard fiberglass long-cane and using material properties to match the harmonic response of the standard cane and optimizing for minimum weight while

maintaining structural stability of the cane body. The inner diameter of the cane was limited by the processor dimensions and could not be smaller than 1.62 cm. The stability of the cane body was a function of the wall thickness and that determined the outside diameter as well as contributing to the total weight of the cane. The optimization was one of minimizing dimensions to reduce the cost and weight of the cane. The outcome of that optimization was used as a constant in the optimization formulas for the electronic collision avoidance system.

The design objective was to maximize user satisfaction. The user satisfaction for the cane was defined as a function of the information quality, weight of the cane, cost, and the operating time on a battery charge.

The cane was modeled as a long, thin cylinder with an ID fixed to 16.2 mm, a size that would accommodate the microprocessor circuitry. The model assumed the cane to be cantilevered at the handle with a maximum force of 14 Newton applied at the tip, perpendicular to the longitudinal axis of the cane. Using the yield stress and Young's modulus for each material, the outer diameter was adjusted to obtain a maximum bending stress equal to the yield stress using the formula:

$$\sigma = M/I/y = 32\ M\ d_o / (\pi(d_o^4 - d_i^4) \qquad (13)$$

where: σ is the bending stress at the handle, M is the moment, the cane length times the perpendicular force, I is the moment of inertia, y is the distance to the centroid, d_o is the outer diameter, and d_i is the inner diameter.

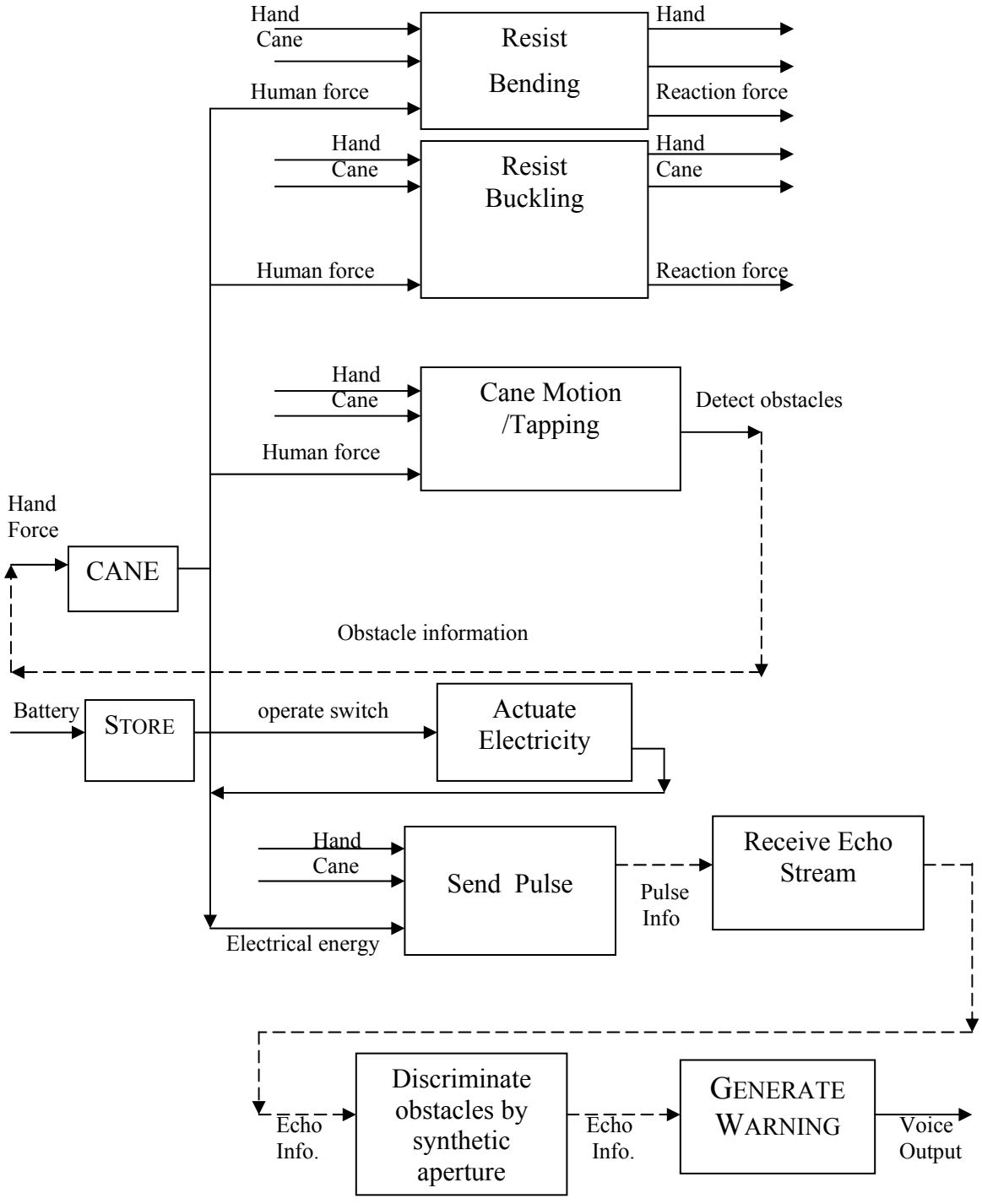

Figure 16: Function Structure Diagram

The mass associated with the above calculated wall thickness was modeled using:

$$m = L\,(d_o^2\pi/4 - d_i^2\,\pi/4)\rho \qquad (14)$$

where: m is the mass, L is the cane length, and ρ is the density.

The critical longitudinal force for buckling was calculated using:

$$P_{cr} = \pi^2 EI/L^2 = \pi^3 E(d_o^4 - d_i^4) / (64L^2) \qquad (15)$$

Where: P_{cr} is the critical longitudinal force for buckling and E is Young's modulus.

Figure 17 presents the relationships of these values for the considered materials.

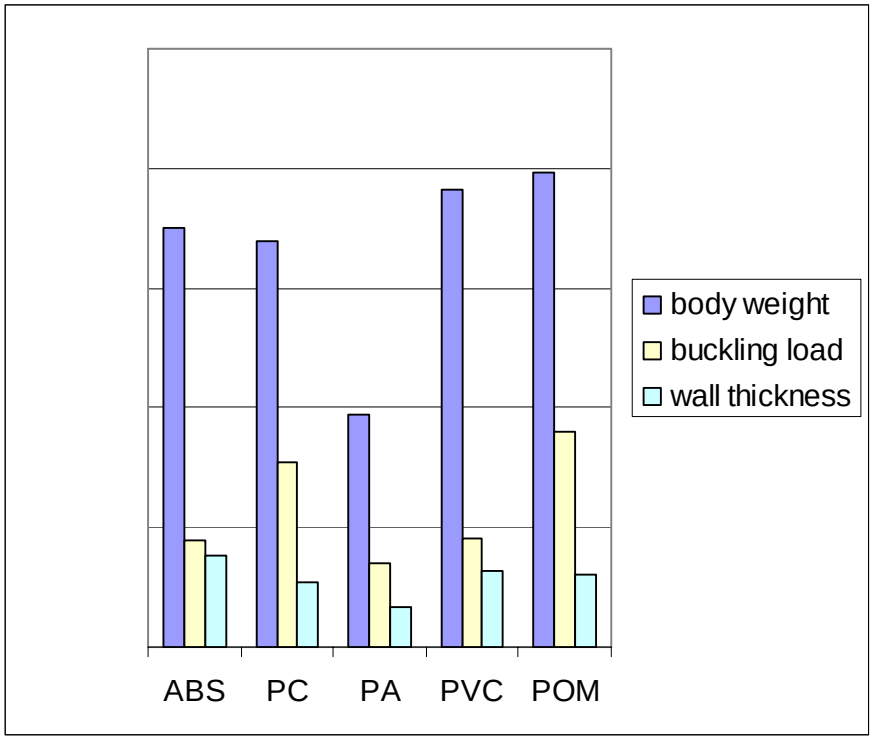

Figure 17: Body weight, buckling load, and Wall thickness to resist max bending stress.

For the design optimization it was assumed that it was possible to produce a cane that can house 1 – 11 sensors. All the sensors were assumed to be of the same weight, to consume the same power, and act as receivers. Receivers add weight and add to the processing load. Three sensors, two receivers and one transmitter, are the minimum needed to form a

synthetic aperture. Additional receivers would provide greater redundancy for obstacle verification but would increase the data processing load, weight, and cost. The increased data processing load would reduce the operating time between battery chargings and the added improvement in information quality would quickly diminish to the point where little would be gained by adding another sensor.

The parameters that define user satisfaction for the electronics, namely information quality and operating time, relate to the number of sensors, the type of algorithm used in the data analysis, and the selection of a battery. This process constitutes the initial design of the electronics.

A Pareto optimal set of feasible choices was formed from the results of material design and electronics design. The choice that optimized the user satisfaction was selected as the final design for the cane. The objective function (user satisfaction function) was defined in terms of the four performance measures of the cane, cost, weight, information quality, and operating time as follows:

C1 *MIPS/13.2 + C2 * 100/cost + C3 * Operating time/10+ C4 * 176 /Weight (16)

The terms C1, C2, C3 and C4 represent the weights attached to the different performance measures and were 0.5, 0.25, 0.15 and 0.1 respectively. (The value of C1 clearly shows that information quality was of prime concern in the design of the cane and hence a large weight was assigned to it.) Dividing a measure by the maximum feasible value of the measure if the measure was to be maximized, or dividing the minimum feasible value by the measure if the measure was to be minimized, normalized the performance measures. The user satisfaction objective function was therefore a value between 0 and 1.

The design variables used to arrive at the above performance measures were:

1) The number of sensors (‘n’) – The possible number of sensors considered for this project was between 1-11
2) Type of algorithm (‘a’) – The algorithm was defined as either 1 or 2 depending on the complexity. The more complex algorithm represented by the number 2 requires twice the number of instructions to implement as the simple one denoted by 1.
3) Battery capacity (‘b’) - Was a set of discrete values based on commercial battery sizes.
4) MIPS was defined by the following relation:

$$0.6\ n\ a \tag{17}$$

5) Operating time was defined as:

$$b/0.195\ \text{MIPS} \tag{18}$$

6) Cost was defined as follows:

$$\text{Cost of battery} + \pi\ d\ t\ \rho\ (\text{Cost of material per gram}) + (\text{Cost of sensor})n \tag{19}$$

where: $\pi = 3.14$, d = mean diameter of the cane, t = wall thickness, and ρ = density of the material (2.7 gm/cc for aluminum), and the cost of a sensor was assumed to be $ 12 .

7) The weight of the cane was calculated as:

$$\pi\ d\ t\ \rho + \text{Weight of the battery} + (\text{Weight of a sensor})n \tag{20}$$

where the weight a sensor was assumed to be 5 gm.

Lithium batteries were found to provide the best performance in terms of power capacity with low weight and small size and they were available commercially in standard, discrete packages. It was necessary therefore, to use quadratic formulas in the

optimization formulas for the electronic collision avoidance system, to model battery weight and cost as a function of lithium battery capacity. However, since the cost per watt-hour of capacity (Figure 18) is much less for the larger AA size battery packages then for the smaller disk batteries, as is the ratio of weight per watt-hour (Figure 19), the optimization results always specified the larger AA size lithium battery.

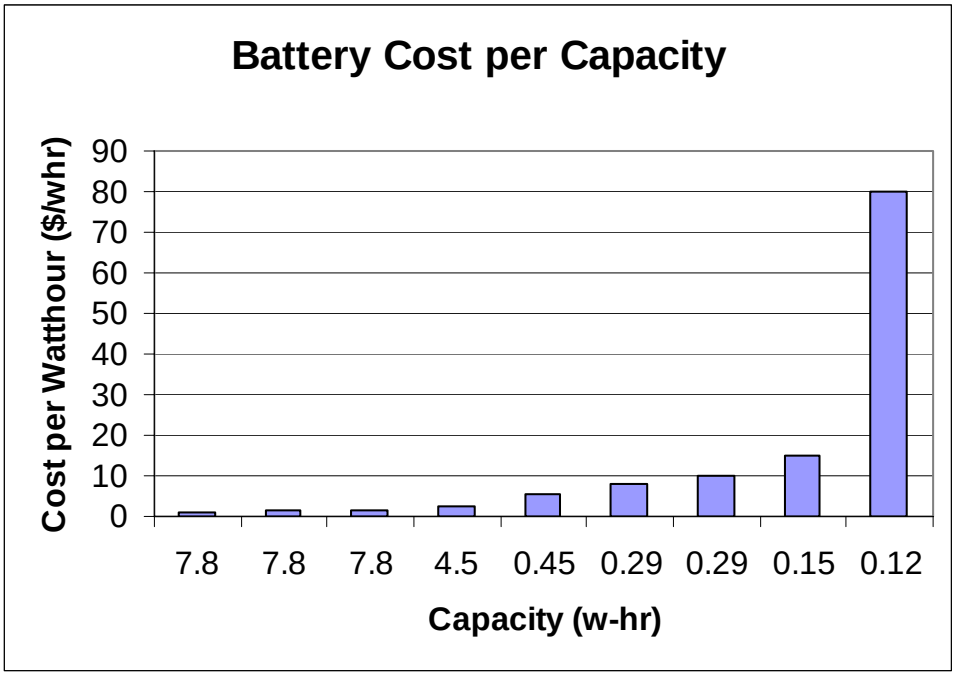

Figure 18: Battery cost as a function of capacity.

The final optimized design was a tradeoff between the conflicting objectives of low cost and high information quality. The design optimization of the cane body was bounded by the characteristics of the standard fiberglass cane, selecting the material that would provide the desired mechanical response and the needed structural stability with the minimum weight, cost and outer diameter. The electronic collision avoidance system configuration selected by optimizing user satisfaction, used 3 sensors with the more

complex type 2 algorithm. The results of the optimization are presented in Figure 20 and show a peak in user satisfaction (US) using 3 sensors.

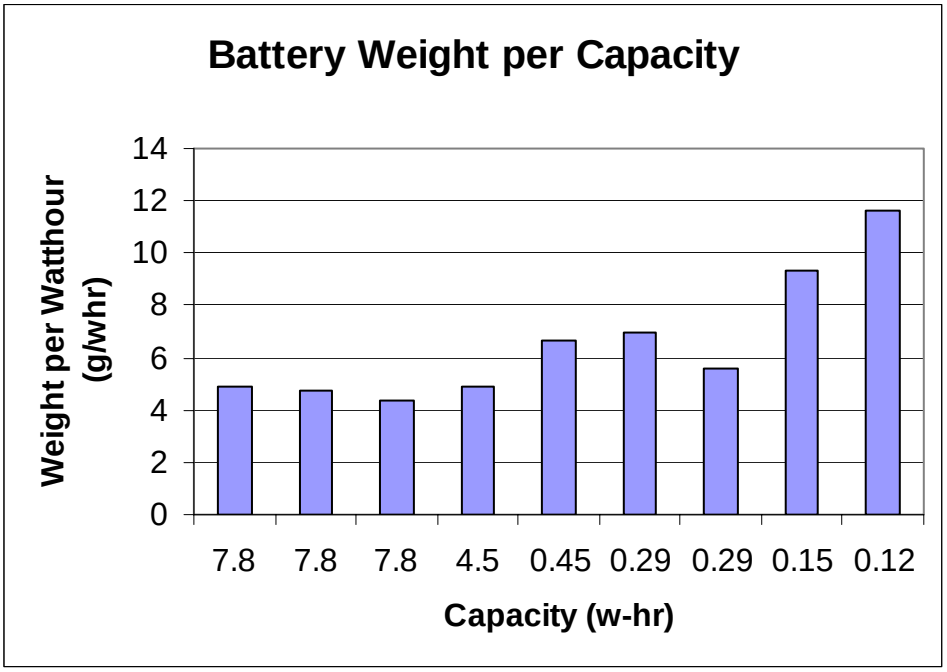

Figure 19: Battery weight as a function of capacity.

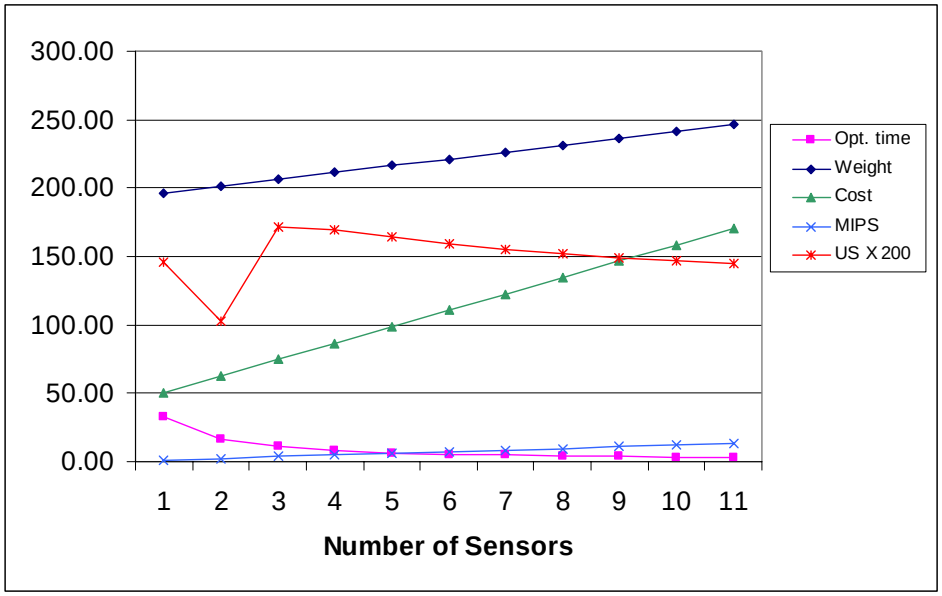

Figure 20: Optimization Results

3.2.4 Material Selection

The structural design of the cane involved selection of materials and wall thickness to resist the expected loads the cane would be subjected to while minimizing the weight and cost. Mechatronic design principles also required consideration of the human factors to ensure the proper feel of the cane. With the complicated geometry required to mount and house the ultrasonic sensors and circuitry, injection molding was considered as the probable production process and the final material choices were made accordingly. The dimensions of the cane were optimized for each material to arrive at the final dimensions of the cane.

A standard long-cane of polyester fiberglass construction was modeled in Pro-Mechanica. E-glass filled polyester was the fiberglass material chosen to model the standard cane. To match the response or 'feel' of the standard long-cane the Cambridge Engineering Selector (CES) was used to identify materials with a similar loss coefficient

to E-glass filled polyester. Having a similar loss coefficient would ensure the vibrations would travel analogously through the canes. This would indicate that if the canes experienced a similar first quantitative frequency mode, subsequent modes would also be equal. Potential materials were woods, polymers, and glass-filled polymers such as acrylonitrile butadiene styrene (ABS) and polyethersulphone (PES).

The equation for the resonant frequency of a tube (Equation 20) was used to select

$$F_1 = \frac{C_1}{2\pi}\sqrt{\frac{EI}{\rho A \cdot l^4}} \tag{21}$$

materials that would have a similar frequency response to the polyester white cane. In this equation the material properties composed a constant, $\frac{EI}{\rho A}$, that could be used to match the frequency response, where E is elastic modulus, I is moment of inertia, ρ is density, A is cross sectional area, l is length, C_1 is a constant and F_1 is the first mode of frequency [32]. If the materials chosen for the cane were required to have the same loss coefficient as the polyester-fiberglass used in the standard cane, the value of $\frac{EI}{\rho A}$ had to be held constant to obtain similar frequencies. This was done in order to calculate an appropriate value of the material index $\frac{E}{\rho}$ for the upper and lower portions of the cane in accordance with their dimensions. The geometry of the cane, specifically the cross-sectional area, influences the modes of vibration.

From the material analysis conducted using the frequency equation and the established material indexes, the difference in diameter of the handle and upper body compared with the tapered lower section of the sensor embedded long-cane indicated the use of different

Table 2: Material Properties for Potential Materials for the Cane Body

Section	Material	Loss Coefficient	Elastic Modulus (GPa)	Density (kg/m^3)	E/ρ ($Gpa/kg/m^3$)
Upper	Bamboo (Transverse)	0.01200	1.5000	712.5	0.002105
	ABS (Injection Molding)	0.01527	2.2100	1050	0.002105
	PVC (Rigid Molding)	0.00966	2.9470	1400	0.002105
Lower	POM (20% Glass Homo-Polymer)	0.01035	6.2324	1540	0.004047
	PA (Type 66, 13% Glass Fiber)	0.01268	4.9373	1220	0.004047
	PC (30% Glass Fibre/2% Silicon)	0.01098	6.0400	1470	0.004109

materials for the two sections to better match the response of the standard fiberglass long-cane. Bamboo, poly vinyl chloride (PVC), and ABS were selected as potential materials for the upper section of the cane and polycarbonate reinforced with 30% glass and 2% silicon (PC), 13% glass-filled polyamide 66 (PA) (Nylon) and 20% glass-filled polyoxymethylene (POM) were selected as potential materials for the lower shaft. Table 2 lists the materials and their pertinent properties.

Figure 21: Model of the Sensor-Embedded Ling-Cane

Combinations modeled for the top/bottom, Figure 21, respectively included ABS/nylon, ABS/PC, ABS/POM, bamboo/PC, bamboo/POM, PVC/PC, and PVC/POM. The material combinations were analyzed using the same Pro-Mechanica analysis as the standard polyester-fiberglass cane. The principle criterion for material selection was that the modes of vibration matched those of the standard polyester-fiberglass cane. The first eight modes of each model are displayed in Table 3. The combinations of materials that best match the standard cane's modes of vibration are ABS/PC, followed by ABS/POM, and ABS/Nylon. Since the modes of vibration were a primary concern of this design, the other material combinations, highlighted in red, were eliminated.

Table 3: Modal Analysis of Different Walking Cane Designs

Material(s)	Type	Mode 1 [Hz]	Mode 2 [Hz]	Mode 3 [Hz]	Mode 4 [Hz]	Mode 5 [Hz]	Mode 6 [Hz]	Mode 7 [Hz]	Mode 8 [Hz]
Polyester	Standard	4.94	4.94	30.90	30.90	86.37	86.38	168.84	168.86
ABS and Nylon	SmartCane	5.27	5.27	31.30	31.31	85.39	85.40	167.36	167.39
ABS and PC	SmartCane	4.93	4.93	31.24	31.25	86.49	86.51	169.90	169.92
ABS and POM	SmartCane	4.80	4.81	30.60	30.60	85.20	85.22	167.39	167.42
Bamboo and PC	SmartCane	4.18	4.18	29.96	29.96	85.57	85.57	170.70	170.70
Bamboo and POM	SmartCane	4.07	4.07	29.32	29.32	84.34	84.34	168.30	168.30
PVC and PC	SmartCane	5.52	5.53	32.10	32.10	86.62	86.64	169.90	170.00
PVC and POM	SmartCane	5.39	5.39	31.47	31.47	85.39	85.40	167.37	167.41

The three remaining potential combinations were then evaluated based on mass, maximum deflection, and cost (Table 4). The secondary parameters were to achieve a mass and deflection similar to those of the standard polyester cane. For both of these restrictions, ABS/PC was better than ABS/Nylon and ABS/POM. The modes of vibration, mass, and maximum deflection of the ABS/PC combination most closely match those of a standard polyester-fiberglass long-cane (Figure 22). Although ABS/PC is more expensive than the other two combinations, it is less costly than polyester.

Table 4: The Mass, Cost and Maximum Deflection of the Selected Cane Materials

Material(s)	Type	Mass [g]	Cost [$]	Maximum Deflection [cm]
Polyester	Standard	256	2.43	2.52
ABS and Nylon	SmartCane	235	0.91	3.722
ABS and PC	SmartCane	265	2.03	2.64
ABS and POM	SmartCane	274	1.04	3.75

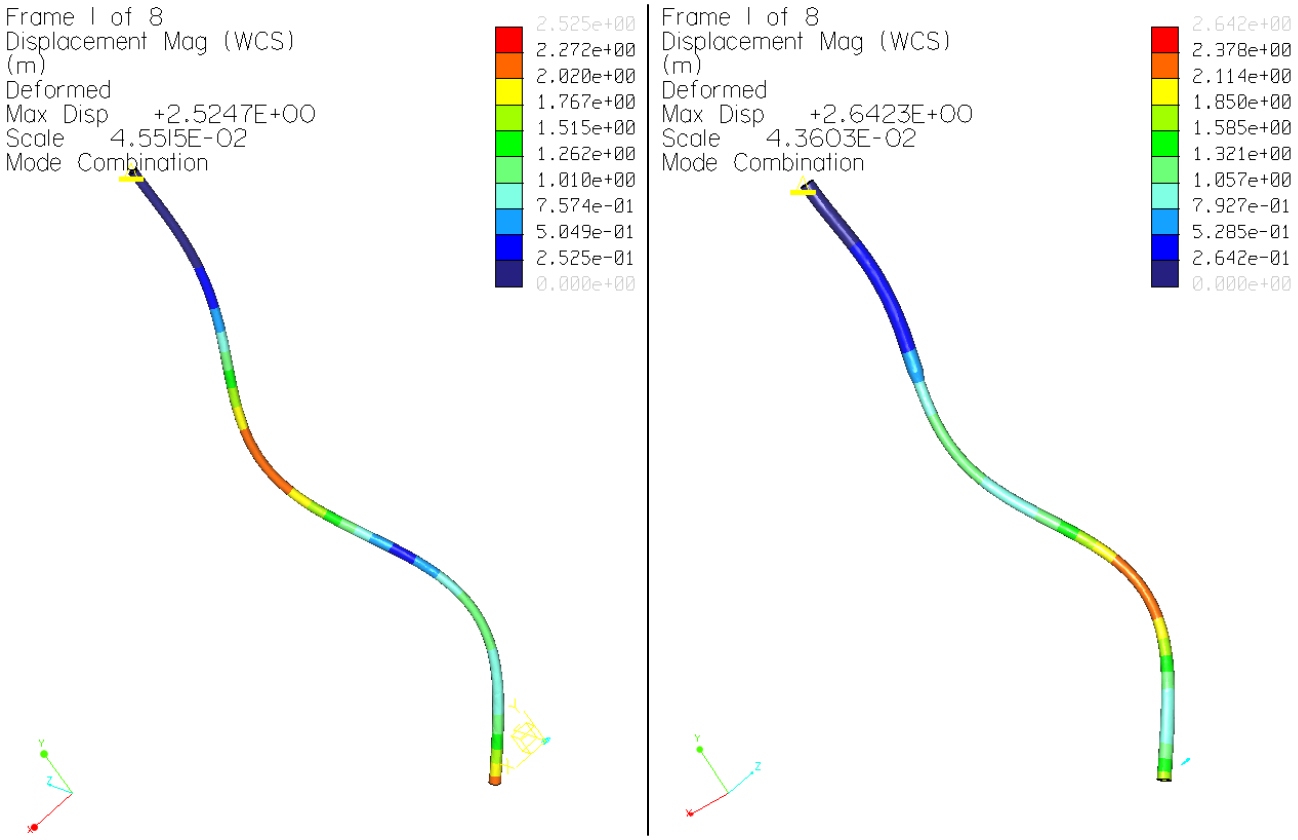

(a) (b)

Figure 22: The deflection and modes of vibration of the standard white cane (a) are most closely matched by the Long-Cane made of ABS and PC (b).

3.2.5 Body Design

The body of the cane was designed as three sections, the Handel and upper section, a transition taper and the cane shaft with end tip. The Handel and upper section housed the batteries, transducers, and PCB. The transition taper joined the upper section to the cane shaft which was replaceable since long canes often get damaged in us by being closed in doors or being stepped on. The ability to replace the cane shaft without replacing the costly upper section of the cane was an appealing attribute to cane users. Figure 23 shows

an orthographic projection and an exploded view 3D rendering of the handle and upper section of the cane. The PCB cover, the battery cap and cover mounting bar are shown in the exploded 3D rendering. The PCB cover both covered and secured the PCB into the cane and the battery cap threaded into the handle to allow easy replacement of the batteries. The mounting bar fit inside the handle adding stiffness and provided attachment points for the cover.

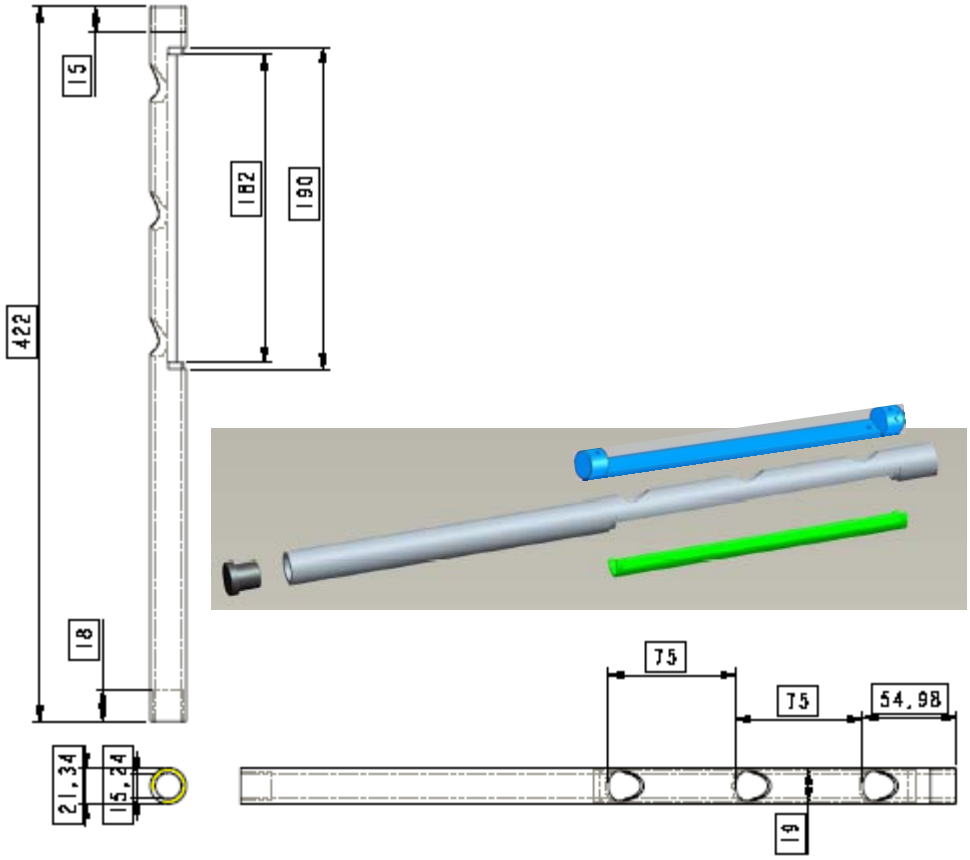

Figure 23: Handle and upper body design.

Figure 24 is a photograph of the transition taper and Figure 25 shows the completed cane side by side with two standard long white canes and with the earlier EMS prototype cane.

From these photographs it can be seen that the design objective of building a sensor integrated long cane that closely resembles a standard long white cane has been accomplished.

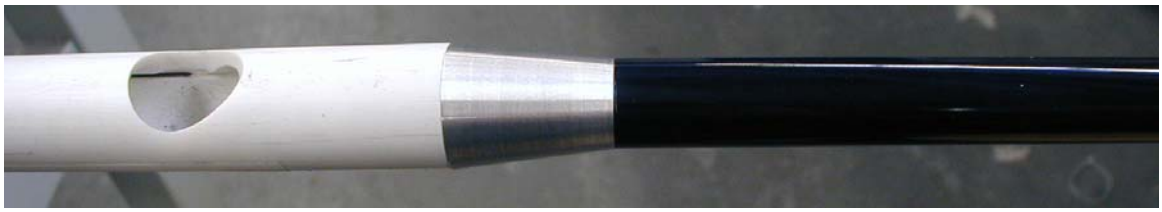

Figure 24: Transition taper connecting the upper section to the cane shaft.

Figure 25: The new cane side-by-side with standard long canes and the earlier EMS cane.

3.3 Sensors and Electronic Circuit Design

The following five basic target requirements for the sensor embedded long-cane's embedded collision detection system were used in selecting the various components to be incorporated into the system design:

(1) detect obstacles that pose a collision threat to the head and upper body of the user, (2) have up to a 4 meters range, (3) not give false alarms, (4) Fit within the body of a long cane, and (5) communicate with the annunciator wirelessly.

These broad requirements demanded a "whole product view" or mechatronic approach to the component selection. Each component or sub-system was chosen to enable the collision detection system meet these requirements.

3.3.1 Transducer selection

The five criteria used in selecting ultrasonic transducers, detection range, sensitivity, beam angle, size, and weather tightness are shown in Table 5 for the transducers considered for the sensor embedded cane. Capacitive transducers were not available in sizes less than 20 mm in diameter and more complicated circuitry was required to interface to them. Therefore all the transducers considered were of the piezoelectric type. The directivity of an ultrasonic transducer increases with its size and operating frequency. On the other hand, Sound attenuation for dry air is proportional to the square of frequency above roughly 10 kHz.[33] This loss due to the compressibility of air renders frequencies above 100 kHz un-usable for a 3 to 4 meter range. The majority of piezoelectric transducers offered for use in air operate at Forty kilohertz and using a higher frequency would require using a higher sampling rate. This makes 40 kHz a good compromise between range and directivity. The best-suited sensors were the SensComp 40KR/T18, 18 mm diameter, 40 KHz solid faced transducer with a 30^{o} beam angle and the SensComp 40 LR/T open faced transducer with a 55^{o} beam angle. Both transducers are a size suitable for mounting on the sensor embedded cane. The

closed-face 40KR18s have the advantage of being environmentally sealed and therefore weatherproof but the open-faced 40LR16s are 5 dB more sensitive and cost less. Both transducers were tested in the final prototype long cane.

Table 5: Ultrasonic transducer selection.

Manufacture	Model	Frequency	Sensitivity	Beam Angle	Face	Size	Price
SensComp	40LR/T16	40 kHz	-70 dB	55^o	open	16.2D X 12 mm	$6.30
SensComp	40KR/T18	40 kHz	-65 dB	30^o	sealed	18D X 12 mm	$10.50
SensComp	40LR/T10	40 kHz	-70 dB	72^o	open	10D X 8 mm	$6.30
SensComp	40KR/T08	40 kHz	-80 dB	125^o	sealed	8D X 5 mm	$10.50
muRata	MA40E7R/S	40 kHz	-74 dB	100^o	sealed	18D X 12 mm	$17.49
Durham Inst.	TR-2436	150 kHz	-83 dBV	32^o	sealed	18.2D X 10.2 mm	$55.00

3.3.2 Sensor spacing

The choice of receiver spacing is a good application of the mechatronics approach to design. A greater spacing between the receivers provides better resolution of the synthetic aperture. This was shown previously by Equation 7. However, the receivers are directional and have a total beam angle of around 30^o for the closed face transducers. The aperture of the sensor array is the overlap of the detection zones of the two receivers. The area between the receivers that is outside this aperture is a dead-zone where an obstacle cannot be seen by either receiver. The greater the spacing between the receivers, the further out the central dead zone extends. The area on either side of the detection zone that can only be seen by one receiver is also a dead zone that is proportional to receiver spacing. Figure 26 illustrates the dead-zone effect. The aperture of the array is the double crosshatched area in the figure.

Receiver spacing also affects the computational load on the embedded processor. Since greater spacing would result in greater angle resolution, greater spacing would translate into more data points to be checked for receiver correspondence. That would demand a faster processor, requiring more power. Also, the sensor spacing would impact the space available in the body of the cane for the circuit boards.

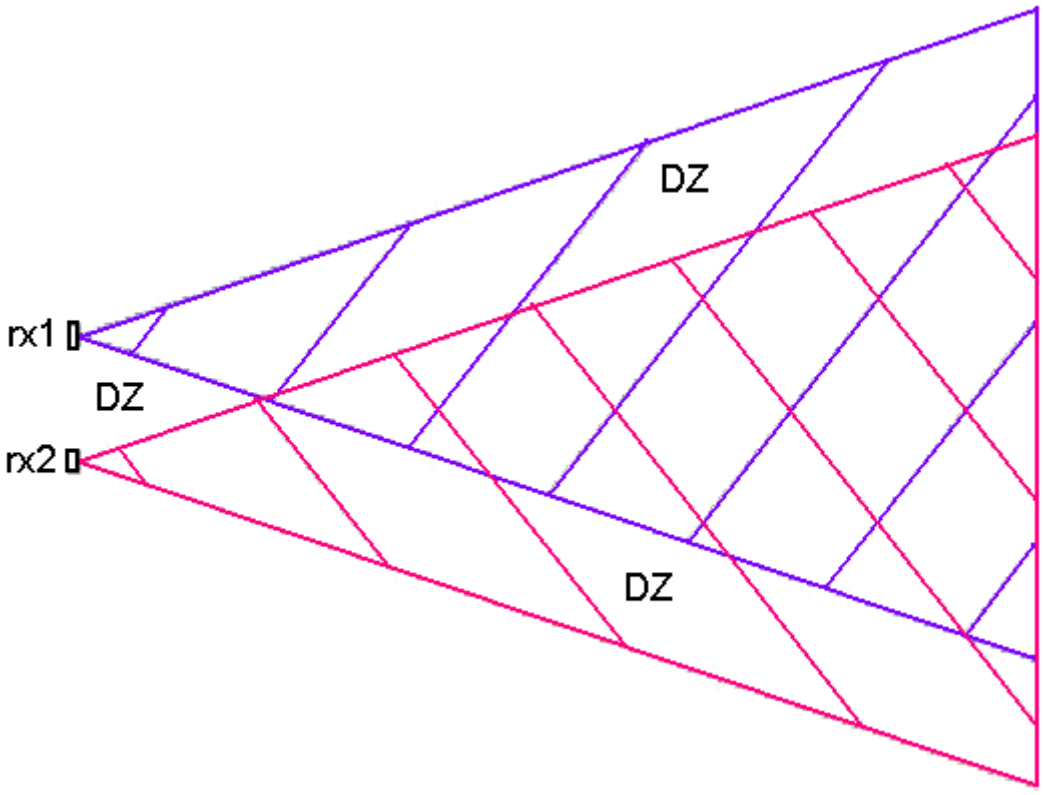

Figure 26: The effect of receiver spacing on dead-zone.

Optimum sensor spacing, therefore, is a compromise between the angle resolution of the array, the size of the detection dead-zone, the circuit board size, and the clock speed of the microcontroller.

The 15 cm spacing used in the design is the result of this design compromise. Prior research has shown that the accuracy of angle measurement and therefore distance measurement is greatly reduced for a relative sensor spacing of less than 14 cm [2]. The dead-zone between the receivers for this spacing is only 28 cm, less than the 1 meter minimum range required, and the maximum sample difference for an in-aperture obstacle at a 150 kHz sample rate is 65 samples.

3.3.3 Microcontroller Selection

Microcontroller selection for the sensor embedded long-cane required an analysis of the available microcontrollers in the marketplace to find the models that met the minimum requirements for processing power, speed, memory, and onboard peripherals. An analog to digital converter (ADC) channel was required for each receiver. A pulse width modulator was needed to produce the encoded pulse to drive the transmitter. A system clock and timers were needed to control the sequence of operation, a port was needed to connect to the transmitter module for output display and memory was needed to store the collected data and perform the necessary calculations. A microcontroller with the necessary peripherals on board would exclude the need for external circuits, reducing the size, complexity, power requirements, and cost of the electronic module as dictated by mechatronic design principles. The processing intensive task of correlation was beyond the capability of standard microcontrollers so the new generation of DSP microcontrollers that recently became available and have the necessary computational power along with the added on board peripherals necessary to drive the ultrasonic obstacle detection system were considered.

The first requirement, processing capability measured in millions of instructions per second (MIPS) or processor clock speed was governed by the sampling rate of the ADC and the real time analysis of the collected data. Capturing the data and performing the analysis in real time was estimated to require 25 MIPS per receiver and the other overhead processes would require several MIPS more. A design with two receivers for obstacle detection would require more than 50 MIPS.

The amount of memory needed was directly related to the ADC sampling rate which was bounded by the by the Nyquist rate for the 40 KHz ultrasonic signal to be sampled and available memory. The upper bound of the sampling rate, f_s, is expressed by

$$f_S \leq \frac{V_S \cdot M}{2 \cdot L \cdot n_R \cdot n_B} \tag{22}$$

where V_S = 343.2 m/s is the speed of sound in air, M is memory size, L is the difference between max and min detection range, n_R = 2 is the number receivers, and n_B is the number of bytes in a data sample. Considering, as an example, that the DSP56F8365 DSP microcontroller provided 32 KB of random access data memory, each data sample occupied 6 bytes of memory for storage and processing, and an L of 3 m was desired for the detection range from 1 m to 4 m, a maximum sampling frequency of 152 kHz would be allowed. In this case, a sampling frequency of 150 kHz was chosen.

A major constraint for selecting the microcontroller was size. The microcontroller had to fit inside the body of the long-cane so the width of the module had to be less then 17 mm. Power consumption and operating voltage were also considered for reducing the demand on the batteries both in size and capacity, which translate into weight. Low cost was necessary to keep the sensor embedded long-cane affordable.

Another important consideration was vender support. The availability of development tools and an in-circuit emulator would reduce the time and effort required to implement the software-hardware system. Table 6 is a comparison of some of the most important features of the considered DSP microcontrollers.

Table 6: Important microcontroller features.

Microcontroller	MIPS	ROM	RAM	A/D	Voltage	Size (mm)	PWM	Power (W)	COST
freescale DSP56F801	40	16K	2K	8 X 12 bit	3.3	9 X 9	6	0.396	$5.95
freescale DSP56F8365	60	576K	36K	16 X 12 bit	3.3	22 X 16	12	0.624	$16.99
Microchip dsPIC33F	40	128K	16K	8 X 12 bit	2.5 - 5	12 X 12	8	0.296	$5.38
Ti TMS320F2809	100	256K	36K	16 X 12 bit	3.3	16.2 X 16.2	16	0.908	$14.78

The Freescale Semiconductor DSP56F8365 microcontroller met the minimum requirements for small size, and sufficient processing power to perform the crosscorrelation for two receivers in real time [30]. This hybrid microcontroller runs at 60 MIPs, has a 12 channel pulse width modulator (PWM), 16 channel A/D converter , 32 KB of Data random access memory (RAM), 512 KB of program flash memory, and it comes in a 22 X 16 mm package that will fit on an 18 mm wide circuit board. Other DSP microcontrollers that met the technical requirements required more power to operate, were too large to fit on an 18 mm wide PCB or were not yet available when the selection was made. For this reason the DSP56F8365 was chosen for this design. In addition, freescale offered a strong array of support and development tools for the DSP56F8365.

3.3.4 Wireless Communication

Size, power consumption and software support were all a consideration in selecting the wireless transceiver for the sensor embedded long cane. Another consideration was the

possible future use of the wireless communication component for controlling doors and traffic lights. For these reasons the IEEE®802.15.4 Standard known as ZigBee was chosen for the wireless communication component of the sensor embedded long cane. The freescale MC13191 is a short range, low power, transceiver that operates in the 2.4 GHz Industrial, Scientific, and Medical (ISM) band and supports the IEEE®802.15.4 Standard. This transceiver is offered by the same vendor as the selected DSP microcontroller and is supported by freescale's 802.15.4 MAC software. The MC13191 is only 6 mm square and draws 37 ma when receiving, 30 ma transmitting and 0.5 ma when idle.

3.3.5 Other Circuit Design Considerations

A block diagram of the collision detection system showing the microcontroller and supporting peripheral components is presented in Figure 27. Key components include a freescale MA7260 3-axis, low-G accelerometer for tilt angle measurement (α in Figure 9), the 2.5 GHz transceiver for communication with the annunciator, active band pass filters/preamplifiers for the receivers, a JTAG interface for programming, and a very low dropout voltage regulator to maximize battery life. The active band pass filter is a single op-amp filter with a center frequency of 40 KHz, a 10 KHz bandwidth, and a gain of 10. The preamplifier is an op-amp with a gain of 10 for a total gain of 100. The transmitter is driven through buffers by two complimentary PWM outputs to reverse the polarity for each half cycle and effectively double the applied excitation voltage.

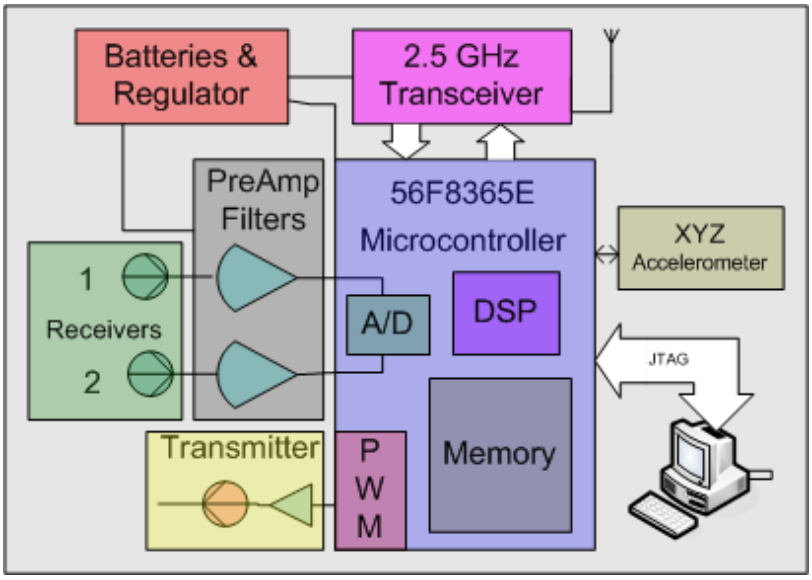

Figure 27: Circuit block diagram for collision detector.

To minimize the cost of manufacture, a 2 layer circuit board was painstaking laid out using OrCAD Layout, placing all the components and routing of the connections on just the top and bottom of the printed circuit board (PCB). Figure 28 shows the layout of the top side of the PCB and the PCB installed in the cane.

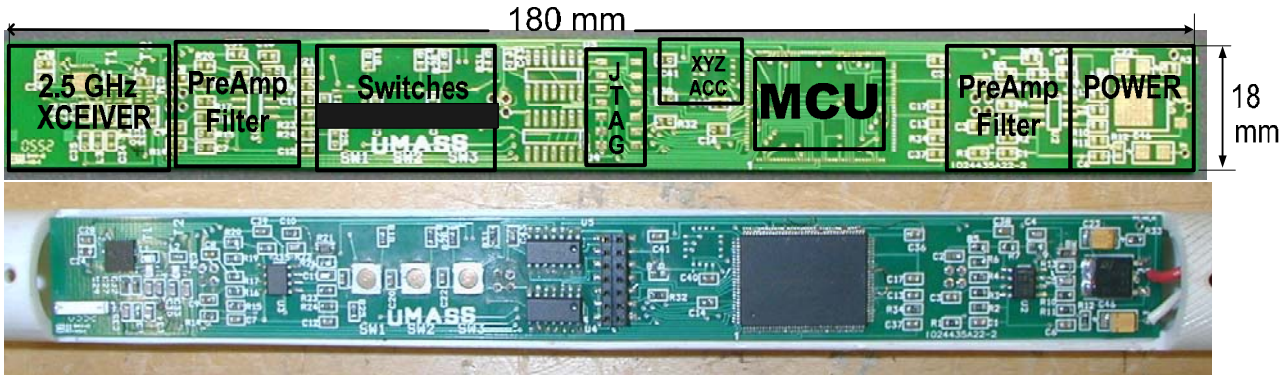

Figure 28: Layout of the Cane PCB and the PCB mounted in the cane.

3.3.6 Embedded Software Design

Both the sensor electronics in the cane and the annunciator electronics are microcontroller based and therefore software driven. Figure 29 presents a flowchart of

the overall function of the software that runs the sensor board in the cane. The initialization sets the sample rate for the A/D converters, sets up the PWM and initializes the transceiver, control registers, and the other parameters. The next block generates a transmit pulse to excite the transmitter transducer. The A/D converters then take 2600 samples at the 150 kHz sampling rate to capture any echoes from objects between 1 and 4 meters distant. The receiver data is cross-correlated with stored echo image to find echoes in the received signal. The correlation peaks are then located using an iterative peak finding algorithm. The correlation peak positions from receiver 1 are then compared to the peak positions from receiver 2 and if they collaborate within the synthetic aperture,

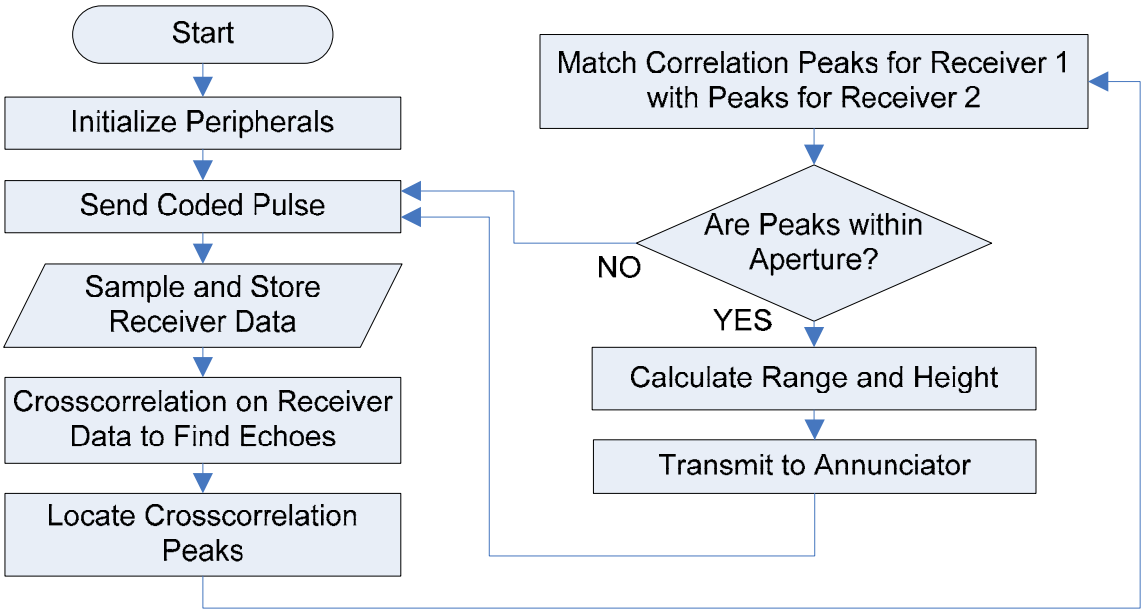

Figure 29: Sensor board program overview flowchart.

the range and height are calculated and the data is sent in numeric form to the annunciator. The annunciator converts the data to a synthesized voice through a look-up table. The process repeats until the cane is shut off.

The transmit pulse was generated by programming the PWM to output 4 cycles at 40 kHz for each digit of the binary encoding number. The polarity or the PWM output was reversed at the 4 cycle boundary if the bit to be encoded was a zero.

The two A/D converters were enabled in triggered mode using a timer set to 150 kHz as the trigger source. Both receivers were simultaneously sampled and the 2600 samples corresponding to the time period when echoes from objects between 1 and 4 meters distant would be received were stored as a two dimensional array in memory.

Cross correlation with a stored image of a high signal to noise ratio echo of the transmitted pulse was performed on the recorded time domain samples and the correlation peaks were located for each receiver by an iterative hill climbing algorithm.

The annunciator software also starts by initializing the registers and peripherals. It then listens for a data transmission from the cane. When data is received, the distance value or error message is used to lookup the prerecorded voice string to warn the user through a speaker or headphones.

The software was written in C and assembly language using the Freescale CodeWarrior™ Development Tools with the Processor Expert Rapid Application Development tool.

3.3.7 Alarm Annunciation

The Sensor Embedded Long-Cane needs to warn the user of potential threats in a timely manner without detracting from the user's perception of the environment or bringing undue attention to the user. These criteria ruled out using beeping tones that would distract the user from listening for the environmental sounds that aid in safe travel. The

time constraint imposed by a normal walking speed of around one meter per second greatly restricts the amount of information that can be communicated. An obstacle detected at a distance of three meters must be reported in less than the three seconds it would take to collide with it. To meet these requirements a synthesized human voice was chosen to warn the user of an impending collision. The synthesized voice will only report the distance to the detected threat to the nearest foot giving warnings such as “seven feet.” This type of annunciation can be performed in less than one second.

In the absence of a threat the system will remain quiet. A simple voice warning of a threat does not require intense concentration to be understood by the user and does not have to be loud enough to draw attention to the user.

CHAPTER 4

EXPERIMENTAL SETUP

The experimental setup underwent several iterations before the cane based system was implemented and tested. First the concept of the coded pulse approach using DSP was modeled in Mat lab and a PC based data acquisition system (DAS) was used to implement and test the correlation and matching algorithms. This setup could generate a transmit pulse encoded with the 13 bit Barker code and perform a correlation on the data from one receiver sampled at 80 kHz but the limited sampling rate of the National Instruments A/D board did not allow sampling two receivers at a high enough rate to test the synthetic aperture. This limitation was overcome when an evaluation board for the targeted microcontroller family was supplied by Motorola (now Freescale) semiconductor and was used to acquire experimental data and perfect the circuit design. Finally the Printed circuit board for embedding into the cane was designed and laid out using a computer aided design (CAD) package, populated with the components and incorporated into the new prototype cane. This integrated system was used to conduct all but the earliest tests presented in this section.

4.1 Testing Done with the Demo Board

The 56F8300DEMO development board was used to test and develop the design. The demo board is a 5.5 by 5.5 inch PCB with a 56F8323 DSP hybrid microcontroller with all of its I/O ports and peripheral devices accessible through header pins connectors on the board and a JTAG port to connect to a PC for programming and debugging. Two receiver transducers and a transmitter transducer were mounted in a polycarbonate fixture as

shown in Figure 30. The fixture surface was angled at 34^{o}, the nominal angle of a long-cane in use. The axes of the transducers were at an angle of 60^{o} with respect to the fixture surface to simulate their mounting in the cane. This mounting arrangement puts the area of interest for obstacle detection within the physical aperture of the transducers and duplicates the mounting arrangement in the long-cane.

The transmitter was connected through an inverting buffer to the PWM output of the

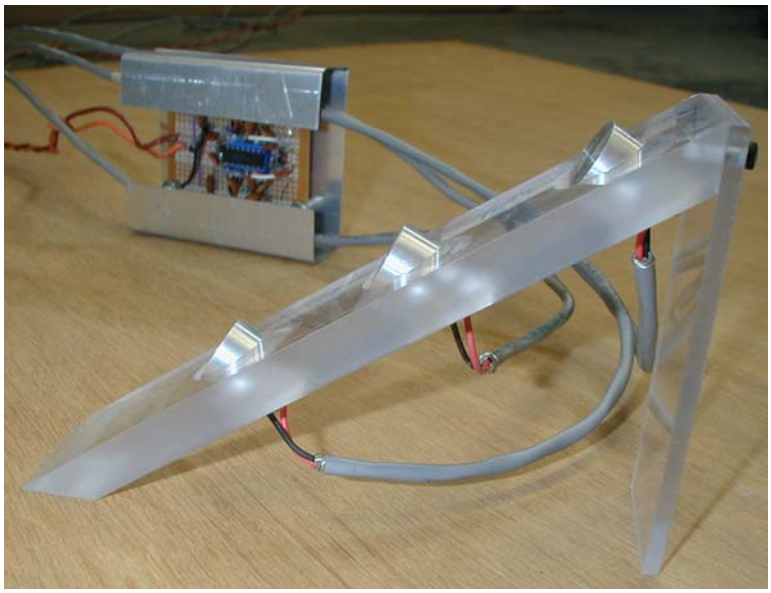

Figure 30: Mounting of transducers for lab testing.

56F8323 microcontroller and the receivers were connected to two of the A/D inputs through the active band pass filters and preamps seen in the photograph.

The CodeWarrior development system running on a personal computer was used to program and communicate with the microcontroller. A 91 x 102 cm board was used as a target to obtain echoes with a 10 dB signal-to-noise ratio, similar to Figure 7, for each receiver to use as correlation vectors. Various obstacle arrangements were then used to test the response of the system and the ability of the synthetic aperture to discriminate for

obstacles in the path of interest. The 56F8323 only has 8 KB of data RAM which is enough memory to store 1500 sample points from each receiver but not enough to perform the correlation on the data. The CodeWarrior development tools were used to write a program in C to use the PWM to transmit the coded pulse and to sample the two receivers with the A/D converters. To process the data it was necessary to export the contents of Data Ram using the CodeWarrior debugger to an Excel spread sheet where it could be manipulated and plotted. Another spread sheet was set up to perform the correlation. The C code to perform correlation and the synthetic aperture function was developed using Microsoft Visual Studio C. Targets of various sizes were hung from the ceiling in the lab and data was tediously collected to test the algorithms and C code.

4.2 Testing Done with the Prototype Board

The prototype PCB described in section 3.3 was installed into the body of the new cane and connected to the CodeWarrior Development Studio via the JTAG port. A JTAG interface was constructed using the JTAG connector of a DEMO board that had a bad processor. The failed 56F8323 was removed from the DEMO board and the JTAG to parallel port circuitry on the board was utilized to connect to the JTAG interface on the prototype board. The C code developed in Visual Studio C for performing the correlation and synthetic aperture functions was ported to CodeWarrior C where all the trigometric functions use a 16 bit fractional type that is not in the ANSI C standard. Using the CodeWarrior debugger the embedded program for the sensor embedded long cane was tested to insure all functions were behaving as designed and that the algorithms and type conversions were giving correct results. The CodeWarrior windows console, available

when connected to the PC through the JTAG port and running the debugger, was used to display the detailed results of the embedded collision system for testing.

Using the above setup (Figure 31) with the cane body held in a test fixture at an inclination of $34^{o,}$ A series of tests were conducted to measure the accuracy and percent error for detecting various realistic obstacles such as a rectangular plate, a narrow rod, and a ball suspended at different heights and at a range of distances from the cane The results of these tests will be presented in section 5.

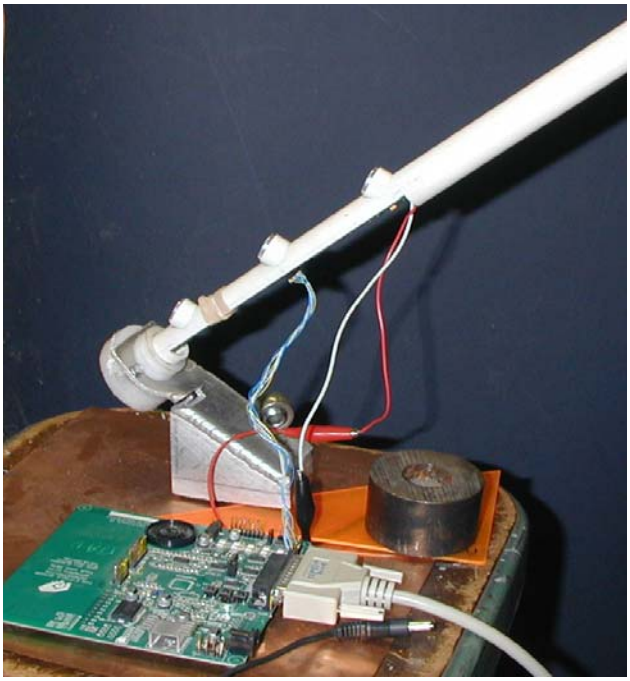

Figure 31: Cane body mounted in a fixture

4.3 Testing Done with the Prototype Board and the Wireless Interface

The protocol and transceiver control software for the IEEE®802.15.4 wireless communication standard was added to the embedded program and debugged using a DLP Design DLP-RF1-Z USB port transceiver (Figure 32) connected to a PC. This provided a known wireless connection to test the wireless communication hardware and software on

the embedded obstacle detection system. Using this setup and a laptop computer as the remote annunciator, a series of field test were conducted to determine the reliability and accuracy of the embedded obstacle warning system.

Figure 32: The DLP Design DLP-RF1-Z USB port transceiver

CHAPTER 5

EXPERIMENTAL RESULTS

5.1 Results for Testing Done with Demo Board

A test was designed to check if the synthetic aperture would detect objects in the area of interest. Three boards simulating obstacles were suspended from the ceiling of the laboratory to test the system (Figure 33). Table 7 lists the size of the presented surface of each obstacle, the range or distance of each obstacle from the transmitter transducer, and the minimum height above the floor. The range of height for each obstacle was the bottom height plus the height of the obstacle. An electrical control box on the bench at the end of the room was also in the range of the transducers and in the detection zone for the synthetic aperture.

The correlated receiver data for this test is presented in Figure 34 with the correlation peaks collaborated by the synthetic aperture highlighted.

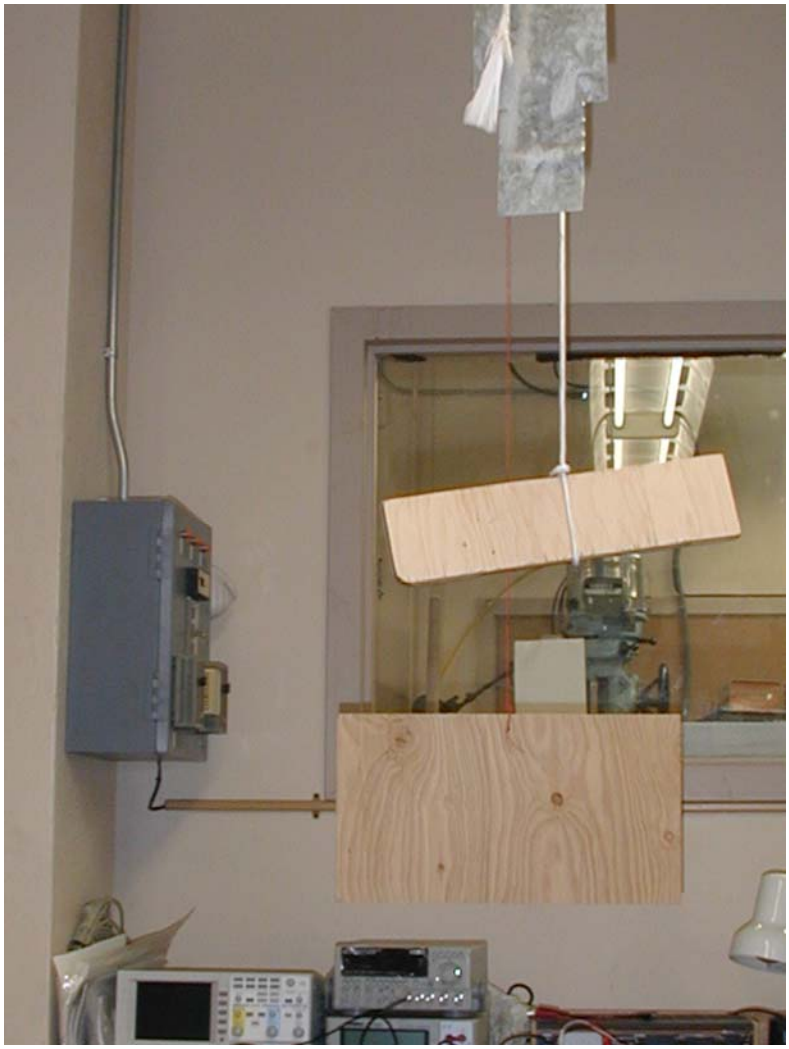

Figure 33: Suspended obstacles in test layout.

Table 7: Test obstacle layout.

Range (m)	Bottom Elevation (m)	Obstacle Height (cm)	Obstacle Width (cm)	Reported Range (m)	Error (%)
1.27	0.76	20	13	1.22	3.9
1.75	1.40	9	36	1.86	6.3
2.39	1.03	25	46	2.34	2.1

The sample numbers on the X axes are equivalent to TOF since the sampling rate is fixed. The Y axes is the relative correlation value, a higher value represents a stronger correlation with the coded transmit pulse.

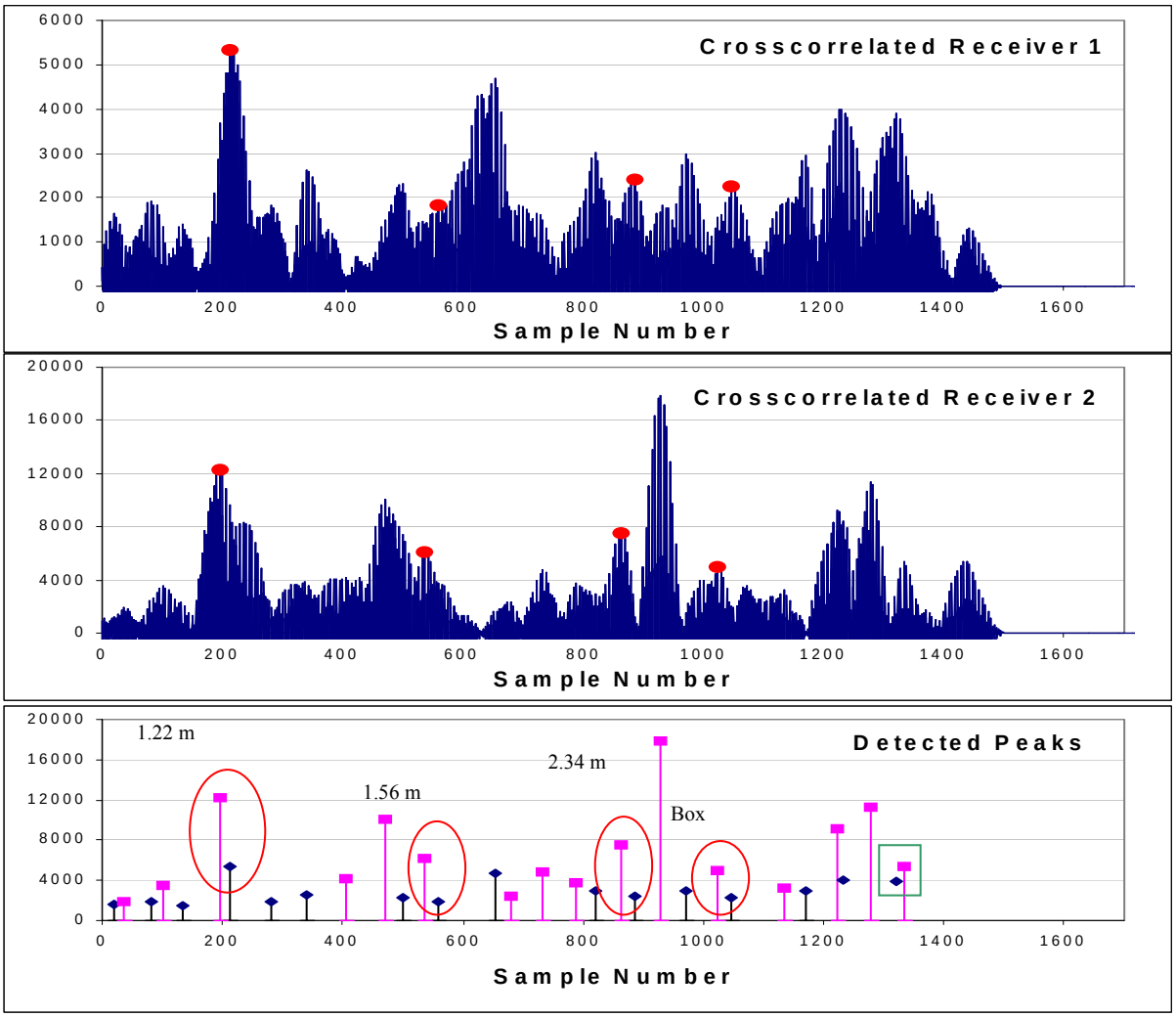

Figure 34: Correlated receiver data showing collaborated peaks.

This figure illustrates how the synthetic aperture algorithm discriminated against all the false and spurious correlation peaks to detect the collaborating peaks for the three obstacles and the box. All three obstacles were detected by the synthetic aperture as well as the electrical box on the bench. The correlation peak pair in the square indicates an

object only 0.58 m high, below the synthetic aperture. The correlation peaks from spurious reflections and echoes from objects outside one of the receiver's aperture and picked up by the other receiver were rejected by the synthetic aperture criteria. When operating in a long-cane, only the closest collision hazard will be reported to the user to allow for evasive action. The crowded small area of the laboratory represents a worst case scenario. The walls, chairs and other item in the room generate numerous spurious reflections of the transmit pulse and therefore is a good test of the synthetic aperture's ability to discriminate against false echoes. Another test was designed to have a strong echo source outside the synthetic aperture and a smaller obstacle in the detection area. Two obstacles were used for this test, the obstacle at 1.65 meters in test 1 and a 0.53 w x 0.66 h board standing on the floor at 2.1 meters. The system reported an object at 1.71 meters but did not report the board outside the synthetic aperture at 2.1 meters even though it presented a larger area to generate a stronger echo.

5.2 Results for Testing Done with the Prototype Board

A 152 mm by 152 mm (6"x 6") plate was suspended at 1.21 meters (4') and 1.52 meters (5') above the floor. The fixture mounted cane body and the computer used to program and monitor the embedded microcontroller were placed on a wheeled cart and the range or distance to the suspended plate was adjusted by moving the cart. The cane was moved in 30 cm (1ft) increments from 1.2 m (4ft) to 3.7 m (12ft) from the suspended target and thirty or more measurements by the embedded obstacle detection system were recorded. Figure 35 shows the experimental setup. The results for the 1.52 meter (5ft) test are presented in Figure 36 and Figure 37. Figure 36 shows the error in

range measurements and Figure 37 displays the error in height measurement. The results for the 1.2 meter (4ft) test are presented in Figure 38 and Figure 39. Figure 38 shows the error in range measurements and Figure 39 displays the error in height measurement.

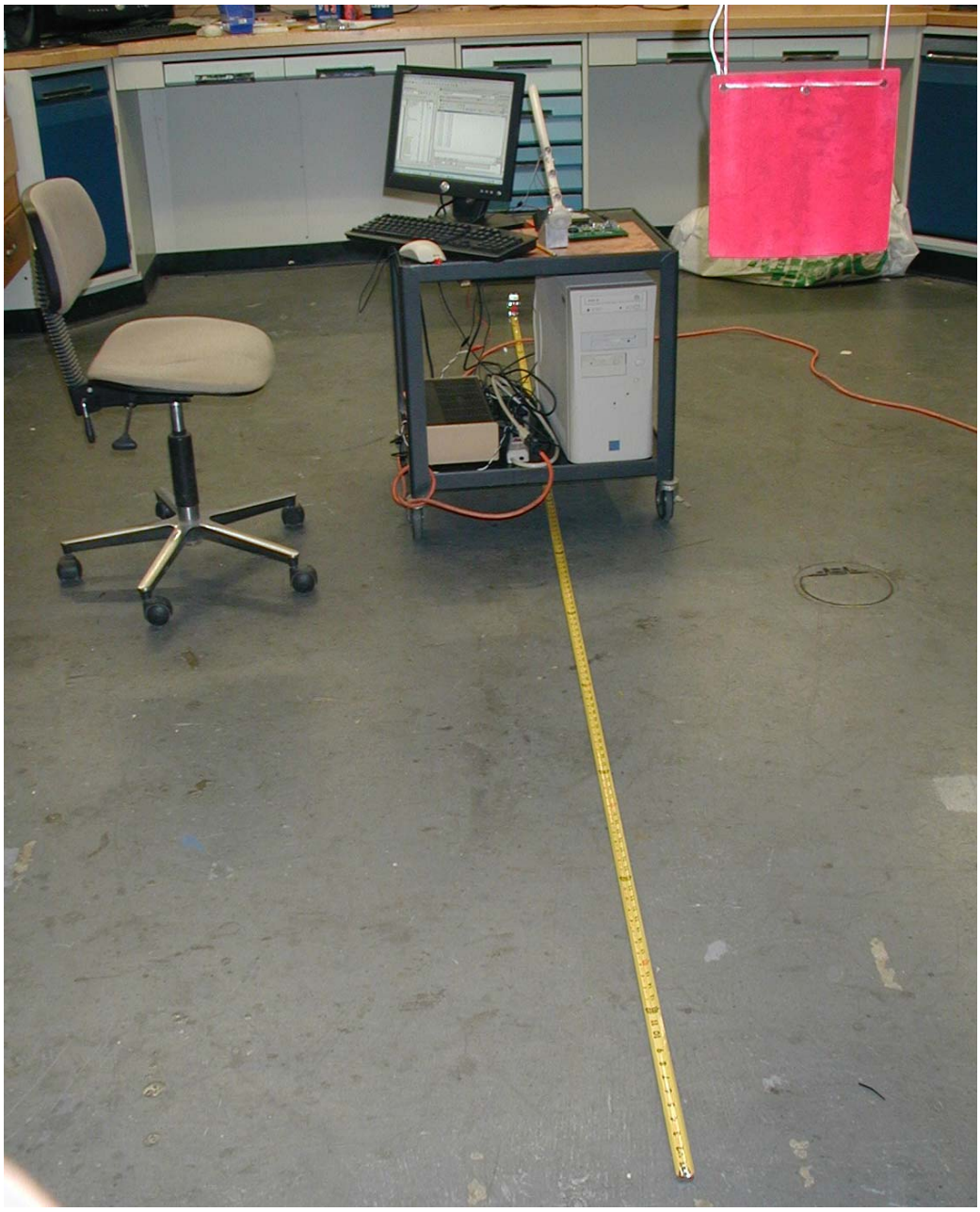

Figure 35: Experimental setup for error calculation.

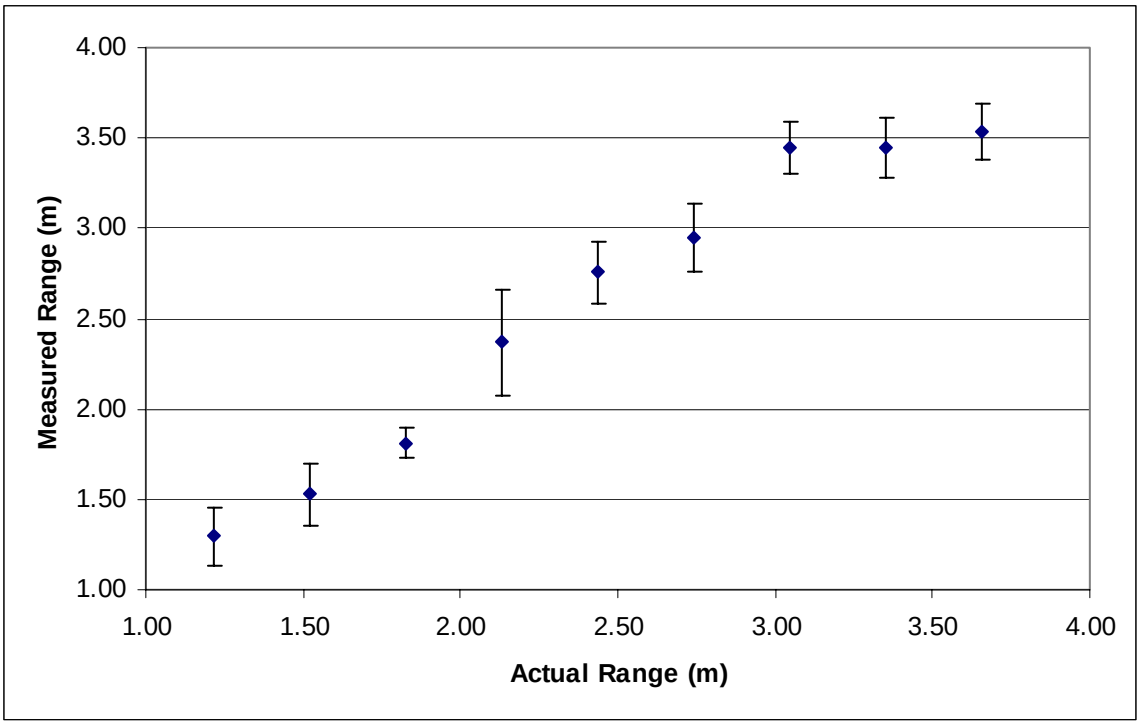

Figure 36: Error in range measurement for target height of 1.52 meters.

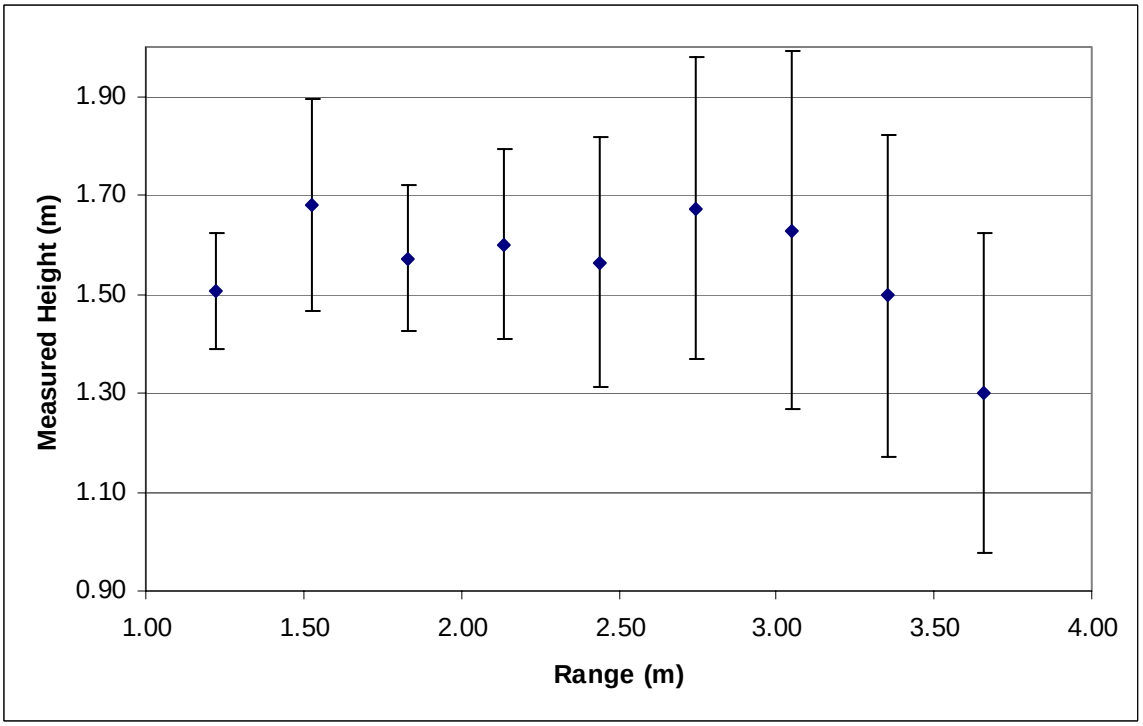

Figure 37: Error in height measurement for target height of 1.52 meters.

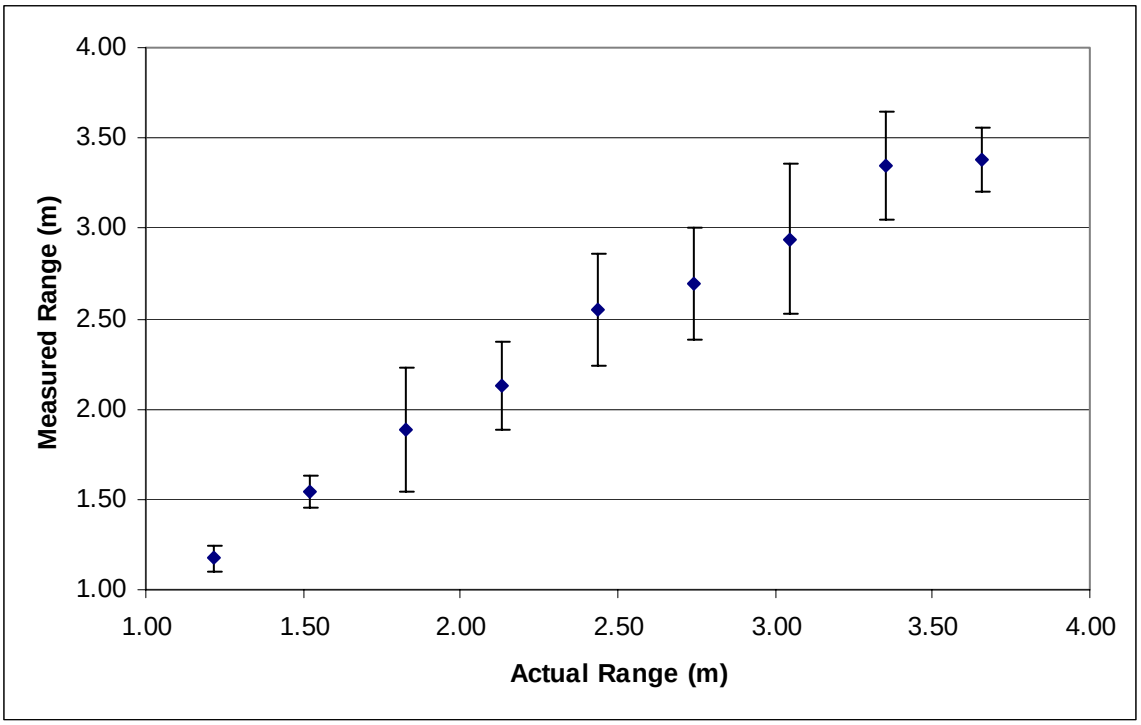

Figure 38: Error in range measurement for target height of 1.2 meters.

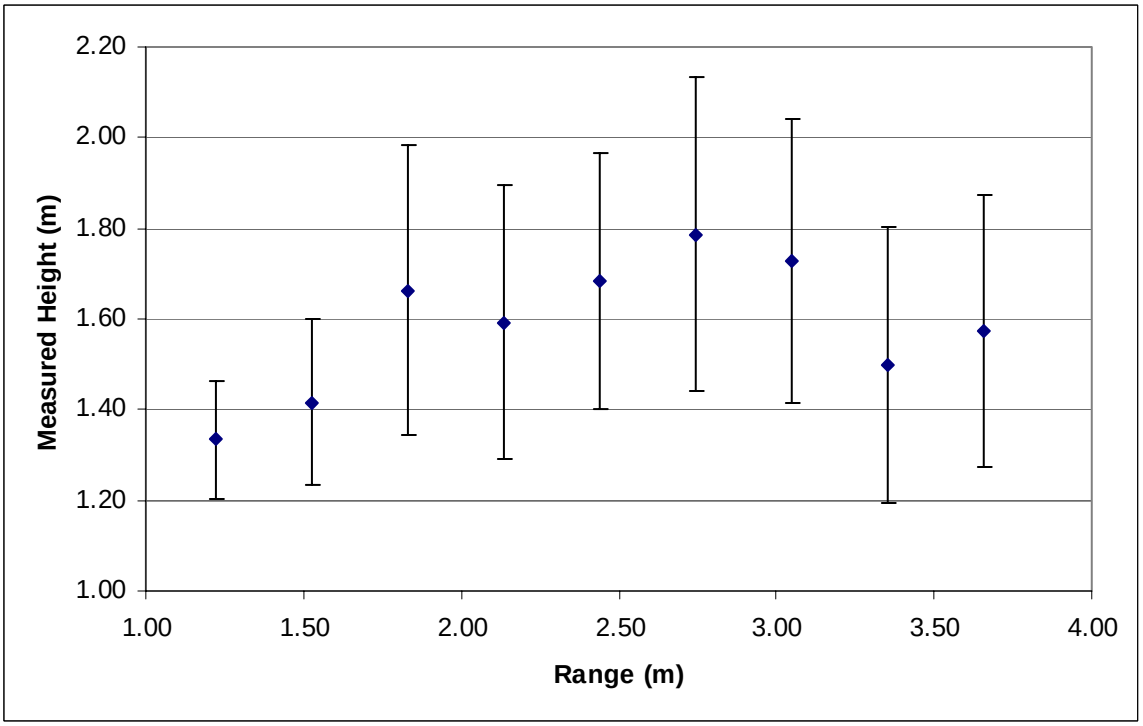

Figure 39: Error in height measurement for target height of 1.2 meters.

The large error bars in the height measurements were a result of the sensitivity of the height measurement to variations in the TOF measurements derived from the correlation peaks. As an example, for an object at a range of 1.75 m and a height of 1 m, a difference of one sample position (the resolution of the system) in the correlation peak for receiver one would change the range measurement by only 6.4 mm but the height measurement would change 39.7 mm. This is at the 150 kHz sampling rate. This had little consequence in the final implementation since the height was only used for internal calculations and was not displayed to the user. Only the distance was given in the warning, and only to the nearest foot, to satisfy the time constraints in real time navigation assistance.

The area of coverage for the embedded obstacle detection system was measured with the same setup but with the cane stationary. The area in front of the transducers was approached from the side at varying distances with a 45 cm X 30 cm (18” x 12”) plate held at a height of around 1.2 meters (4ft) and the position where the embedded obstacle detection system reliably detected the target was recorded. Figure 40 shows the coverage area for the embedded obstacle system.

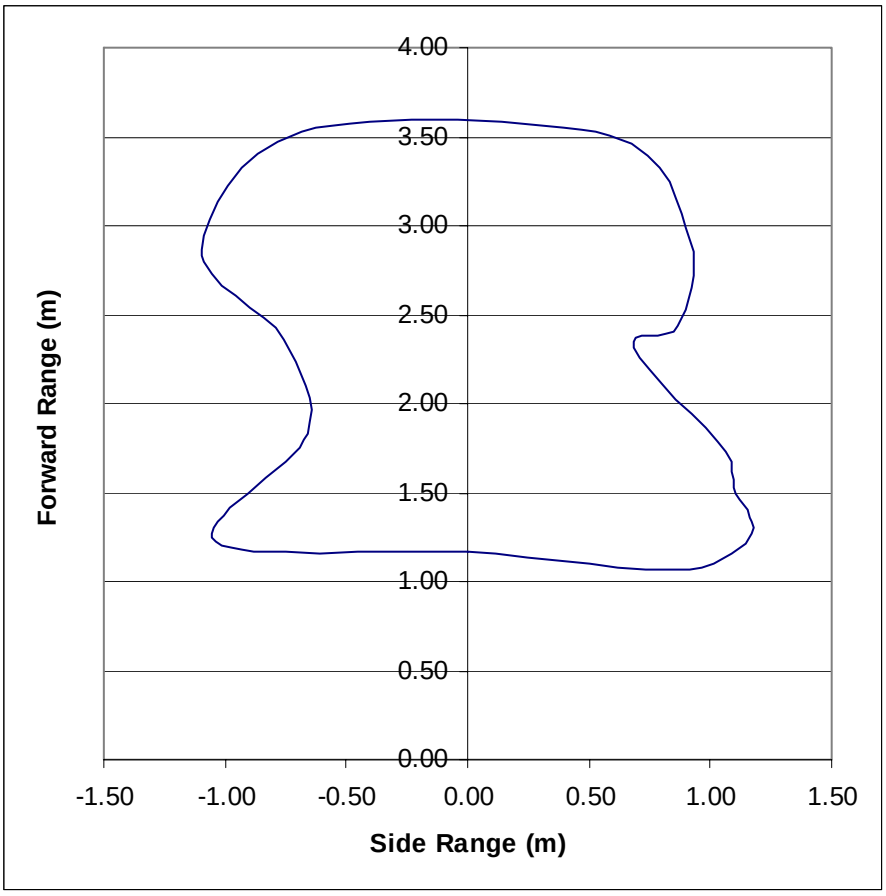

Figure 40: The coverage area for the embedded detection system.

CHAPTER 6

FUTURE WORK

As with most research, the work presented here should precipitate further investigation in four key arrears: Testing of the human factors aspect of the sensor embedded cane in the sight impaired community. Investigating the use of the digital wireless communications capability of the cane to control traffic lights, automatic doors, alarm systems, and other things to aid the sight impaired traveler. Developing a capacitive ultrasonic transducer small enough to fit on the cane to improve the sensitivity of weather tight cane. And to investigate enhanced digital techniques to further enhance the discrimination and identification of week echoes from small obstacles.

6.1 Testing the Ergonomics with the sight impaired community

Beta testing of the sensor embedded long-cane with sight impaired users should be undertaken and the information gained should be used to make design adjustments to the hardware and software design before marketing is begun. A comprehensive testing program should be designed to test the practical and ergonomic aspects of the design. The type of environments that the cane is suitable and practicable to use should be determined as well as the safety limitations for the sensor embedded cane.

6.2 Wireless triggering of traffic control devices

Utilization of the wireless communication capability of the sensor embedded cane to control traffic lights, automatic doors, building access and other conveniences should be investigated to enhance the utility and marketability of the cane. The possibility of adding

GPS functions to the annunciator could also be investigated. To effectively use the ZIGBEE digital wireless protocol to trip traffic lights and automatic doors will require developing a notional or international standard for a communication protocol to interface with traffic control equipment.

6.3 Capacitive Ultrasonic transducers

Capacitive transducers have a better impedance match to air and are therefore more efficient transmitters and more sensitive receivers. They are broadband compared to narrowband piezo-electric transducers which make them more sensitive to noise but able to pass broadbanded encoded signals. [19] In theory, an ideal broadband transducer would not distort the phase of the excitation pulse. This would allow detection of even overlapping echos buried in noise as shown by the simulation results in Figure 41.

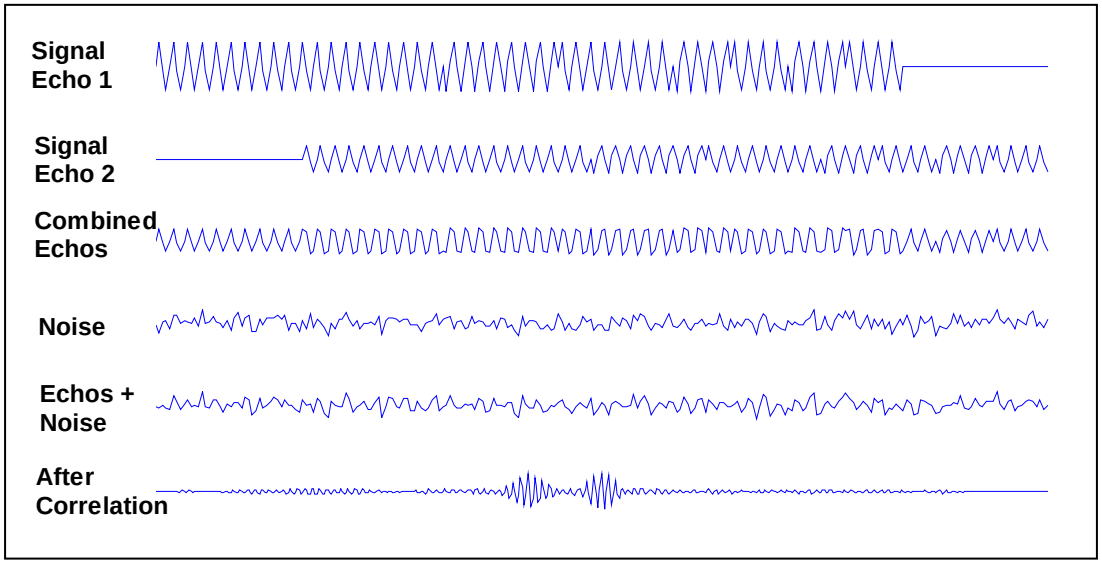

Figure 41: Simulation of the correlation of ideal signal echoes in noise.

The problem is that they are currently only available in a few sizes too large for use on the sensor embedded long cane. The design of a capacitive ultrasonic transducer, suitable for mounting on the cane, should be investigated.

6.4 Enhanced Digital Discrimination Techniques

In combination with capacitive ultrasonic transducers, enhanced digital techniques to further enhance the discrimination and identification of week echoes from small obstacles can be developed using broad banded encoding of the ultrasonic pulse.

CHAPTER 7

INTELLECTUAL CONTRIBUTION AND CONCLUSIONS

7.1 Intellectual Contributions

In this research digital signal processing techniques were applied to develop a method for using encoded ultrasound waves and correlation to improve TOF measurements from the platform of a long-cane.

A filtering algorithm or "*Synthetic Aperture*" was derived to filter correlation peaks and discriminate between obstacles in area of interest and those that do not pose a threat. The "*Synthetic Aperture*" algorithm accomplishes this task with a low computational loading of the microcontroller.

A low power, miniaturized electronic circuit to implement the algorithm from a long-cane platform was developed.

A physical cane housing for the detection system with the *look and feel* of a long-cane was designed to enhance the acceptance of the sensor embedded technology by the sight impaired community.

7.2 Conclusions

Through the efforts of this research significant improvements have been made to the Sensor Embedded Long-Cane in both the mechanical form and the computational detection algorithms areas. A filtering algorithm or "Synthetic Aperture" for the discrimination of obstacles by position and the elimination of false positives was

successfully derived, implemented and tested and a new prototype Sensor Embedded Long-Cane having the look and feel of a standard long cane was developed.

REFERENCES

[1] American Foundation for the Blind, 11 Penn Plaza, Suite 300, New York, NY 10001, http://www.afb.org/

[2] Cai, X., "Long Cane-Integrated Ultrasonic Sensing for Spatial Obstacle Localization", *Doctoral Dissertation*, Dept. of Mechanical & Industrial Engr., University of Massachusetts Amherst, 2000.

[3] World Health Organization, http://www.who.int/pbd/pbl/pbl_home.htm

[4] Kay, L., "Electronic Aids for Blind Persons: an Interdisciplinary Subject", *IEEE Proceedings*, Vol. 131, No. 7, pp. 559-576, 1984.

[5] Heyes, A.D., "The Sonic Pathfinder: A New Electronic Travel Aid", Journal of Visual Impairment and Blindness, Vol. 78, No. 5, pp. 200-202, May, 1984.

[6] Barth, J.L. and Foulhe, E., "Preview: A Neglected Variable in Orienta¬tion and Mobility", Journal of Visual Impairment and Blindness, Vol. 73, No. 2, pp. 41-48, Feb., 1979.

[7] Audenaert, K., Peremus, H., Kawahara, Y., and Van Campenhout, J., "Accurate Ranging of Multiple Objects using Ultrasonic Sensors," Proceedings of e 1992 IEEE International Conference on Robotics and Automation (Nice, France, IEEE, May 1992).

[8] Jorgensen, A.,"Echo Location System for Vision Impaired Persons," US Patent 4907136, 1990 and 5107467, 1992

[9] Ifukube, T., Sasaki, T., and Peng, C., "A Blind Mobility Aid Modeled After Echolocation of Bats", IEEE Transactions on Biomedical Engineer¬ing, Vol. 38, No. 5, pp. 461-465, 1991

[10] Dodds, A.G., Armstrong, J.D., and Shingledecker, C.A., "The Nottingham Obstacle Detector: Development and Evaluation", Journal of Visual Impairment and Blindness, Vol. 75, pp. 203-206, May, 1981.

[11] Hoydai, T., and Zelano, J., "An Alternative Mobility Aid for the Blind: the Ultrasonic Cane", Proc. IEEE 17th Annual Northeast Bioengineering Conference, pp. 158-159, 1991.

[12] Ultrasonic Ranging System Manual, Polaroid Corp

[13] Heyes, A.D., "A Polaroid Ultrasonic Travel Aid for the Blind", Journal of Visual Impairment and Blindness, Vol. 76, pp. 199-201, May, 1982.

[14] Dodds, A.G., Clark-Carter, D., and Howarth, C.I., "The Sonic Pathfind¬er: An Evaluation", Journal of Visual Impairment and Blindness, Vol. 78, No. 5, pp. 206-207, May, 1984.

[15] Audenaert, K., Peremus, H., Kawahara, Y., and Van Campenhout, J., "Accurate Ranging of Multiple Objects using Ultrasonic Sensors," *Proceedings of e 1992 IEEE International Conference on Robotics and Automation* (Nice, France, IEEE, May 1992).

[16] Peremans, H., Audenaert, K., and Van Campenhout, J. M. 1993. A High-Resolution Sensor Based on Tri-aural Perception. *IEEE Transactions on Robotics and Automation* (Ghent, Belgium) 9, 1: 36-48.

[17] Kuc,R. and Siegel, M. W. 1987. Physically Based Simulation Model for Acoustic Sensor Robot Navigation. IEEE Transactions on Pattern Analysis and Machine Intelligence, PAMI_9, 6 (November): 766.

[18] Kleeman, L and Kuc, Roman. 1995. Mobil Robot Sonar for Target Localization and Classification. The International Journal of Robotics Research (MIT) 14, 4 (August): 295.

[19] Webb, P., Gibson, I., and Wykes, C. 1994. Robot Guidance Using Ultrasonic Arrays. Journal of Robotic Systems (Nottingham) 11, 8 (November): 682.

[20] New Wave Instruments, "Glossary – Spread Spectrum & CDMA Technology", http://www.newwaveinstruments.com/resources/glossary.htm

[21] Rudershausen, R., "Synthesis of correlation codes for pulse compression," Symposium on Radar Technology, Munich, West Germany, November 13-15, 1974.

[22] Barker, R. H. "Group Synchronizing of Binary Digital Sequences." In Communication Theory. London: Butterworth, pp. 273-287, 1953.

[23] Sloane, N. J. A. Sequences A091704 in "The On-Line Encyclopedia of Integer Sequences."

[24] Technical specifications for SensComp's 'K' Series Closed Faced Piezo Transducers – 40KR18 and 40KT18, SensComp, Inc., 36704 Commerce Rd., Livonia, Michigan 48150, http://www.senscomp.com

[25] Liu, Jie and Insanna, M. F., "Coded Pulse Excitation for Ultrasonic Strain Imaging,", IEEE Transactions on Ultrasonic, Ferroelectrics, and Frequency Control, Vol. 52, No. 2, February 2005

[26] Webb, P., Gibson, I., and Wykes, C., "Robot Guidance Using Ultrasonic Arrays", *Journal of Robotic Systems,* Nottingham, Volume 11, No. 8, pp. 682, November, 1994.

[27] Sabatini, A, and Rocchi, A., "Digital-Signal-Processing Techniques for the Design of Coded Excitation Sonar Ranging Systems", *Proc. 1996 IEEE International Conference on Robotics and Automation,* Minneapolis, MN, April, 1996.

[28] Rodgers, S. H.. "Ergonomic Design for People at work, Volume 2," Eastman Kodak Co., New York, 1986.

[29] Kuc, R. and Siegel, M. W., "Physically Based Simulation Model for Acoustic Sensor Robot Navigation", *IEEE Transactions on Pattern Analysis and Machine Intelligence*, Vol. PAMI_9, No. 6, pp.766, November, 1987.

[30] Nakahira, K., Okuma, S., Kodama, T., and Furuhashi, T., "The Use of Binary Coded Frequency Shift Keyed Signals for Multiple User Sonar Ranging," Proceedings of the 2004 IEEE International Conference on Networking, Sensing & Control, Taipei, Taiwan, March 21-23, 2004

[31] Ashley S., "Getting a hold on mechatronics", *Mechanical Engineering*, pp.60-63, May 1997

[32] Ashby, Michael, "Materials Selection in Mechanical Design," Butterworth-Heinemann (imprint of Elsevier Health Sciences), pp. 398-399, 1999

[33] Crocker, Malcom J., Handbook of Acoustics, Wiley, N. Y., 1998.